

Schwinger-Keldysh nonperturbative field theory of open quantum systems beyond the Markovian regime: Application to spin-boson and spin-chain-boson models

Felipe Reyes-Osorio,¹ Federico García-Gaitán,¹ David J. Strachan,²
Petr Plecháč,³ Stephen R. Clark,² and Branislav K. Nikolić^{1,*}

¹*Department of Physics and Astronomy, University of Delaware, Newark, DE 19716, USA*

²*H. H. Wills Physics Laboratory, University of Bristol, Bristol, BS8 1TL, United Kingdom*

³*Department of Mathematical Sciences, University of Delaware, Newark, DE 19716, USA*

Open quantum systems pose a formidable challenge for presently available theoretical methods, especially when they contain *many* locally interacting degrees of freedom in *arbitrary* spatial dimension and when dissipative environment imposes *non-Markovian* dynamics on them with memory effects and revival of genuine quantum properties like quantum coherence, correlations, and entanglement. Even the archetypical spin-boson model, where just a single spin- $\frac{1}{2}$ interacts with an infinite bosonic bath, requires switching between methods for different choice of system parameters, temperature of the bath or the need to reach long evolution times. Here, we construct a field-theoretic framework as a *single* methodology that can handle many mutually interacting quantum spins, of arbitrary value S or spatial dimensionality of their geometry [1], as well as for arbitrary system-bath coupling, bath temperature and spectral properties of the bath. Our framework combines Schwinger-Keldysh field theory (SKFT) with two-particle irreducible (2PI) action resumming a class of Feynman diagrams of SKFT to an infinite order. Remarkably, the SKFT+2PI approach closely tracks numerically exact benchmarks obtained from hierarchical equations of motion or tensor network methods for spin-boson in the non-Markovian regime. Such *nonperturbative* features of our SKFT+2PI are traced back to the usage of Feynman diagrams generated by $1/N$ expansion, where N is the number of Schwinger bosons to which the spin is mapped, instead of expansion in system-bath coupling in traditional quantum master equation approaches. Furthermore, we demonstrate the capability of our SKFT+2PI framework to compute two-spin correlators and spin current from them for an anti-ferromagnetic quantum spin chain whose edge spins are coupled to a set of three bosonic baths (one for each spin component) while edge baths are kept at different temperatures—a problem whose complexity can hardly be handled by benchmark methods we used for spin-boson model. The favorable numerical cost of solving integro-differential equations produced by SKFT+2PI framework with increasing number of spins, time steps or spatial dimensionality makes it a promising route for simulation of driven-dissipative systems in quantum computing or quantum magnonics and quantum spintronics in the presence of a single or multiple dissipative environments.

I. INTRODUCTION

The canonical approach to open quantum system dynamics [2–5] formulates quantum master equations (QMEs) in terms of operators. They evolve the reduced density matrix of the subsystem of interest via time-local (i.e., differential) in the case of Markovian [6, 7] regime; or routinely time-nonlocal [8, 9] (i.e., integro-differential) in the case of non-Markovian regime [4, 5, 10]. Formulating time-local QME for non-Markovian dynamics is also possible, but this requires handling additional intricacies [3, 11–13]. The reduced density matrix is obtained by partially tracing, over states in the environmental Hilbert space, the full density matrix of system + environment. For many-body systems, the operators within QME are usually expressed as polynomials of creation/annihilation operators acting in an exponentially increasing Hilbert space, so that a full matrix representation of QME quickly becomes intractable by brute force methods. For example, even for a small number N_S of quantum spins of $S = 1/2$ value or, equivalently,

qubits, the size of matrices $2_S^N \times 2_S^N$ within QME is prohibitively computationally expensive. For Markovian QMEs, where the Hamiltonian operator is quadratic and the dissipative Lindbladian [6, 7] operators are linear in creation/annihilation operators, specialized techniques like “third quantization” [14, 15] can dramatically reduce the computational cost to diagonalizing a $4N_e \times 4N_e$ matrix for N_e fermions instead of a $4^{N_e} \times 4^{N_e}$ matrix required in brute force methods.

The search for efficient algorithms that can solve many-body Lindblad QME beyond quadratic Hamiltonians and with power-law numerical scaling cost [24] has recently led to the development [25] of methods based on Schwinger-Keldysh nonequilibrium quantum field theory [26–29], as well as the equivalent methods in the second-quantization formalism [30]. In particular, functional integral [29] techniques of Schwinger-Keldysh field theory (SKFT) offer a convenient starting point for calculation of various observables and their correlation functions [24, 26], as well as a plethora of field-theoretic tools [29] developed within elementary particle physics. Indeed, SKFT was originally developed for problems in high-energy physics and cosmology [27–29, 31] and later applied to low-energy physics [26]. Such SKFT for open quantum systems has been applied to a number of dis-

* bnikolic@udel.edu

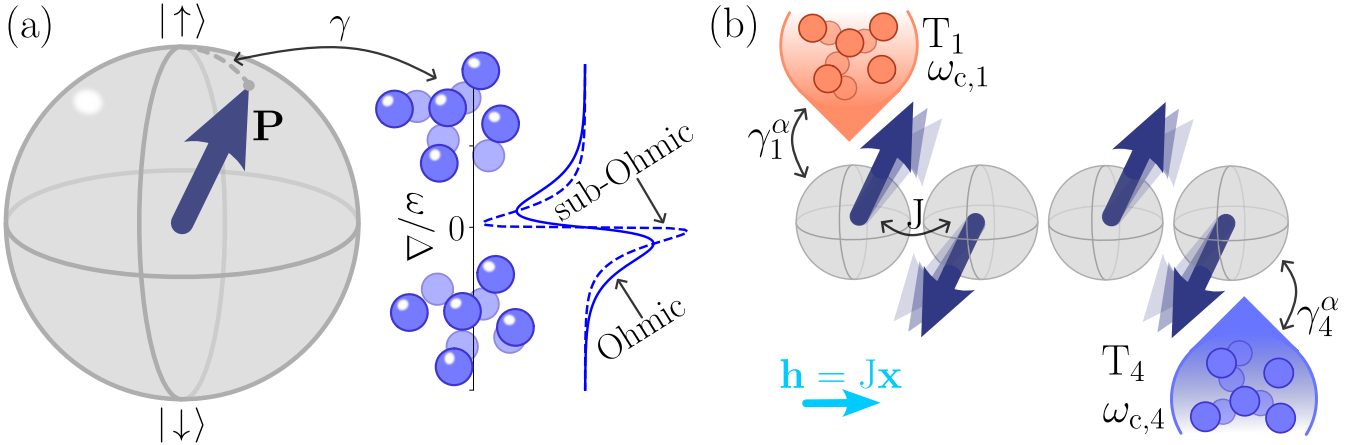


FIG. 1. (a) Illustration of the spin-boson model [Eq. (1)] in which a two-level system, such as spin $S = 1/2$ or a qubit, interacts with a dissipative environment modeled [16] as a bath of bosons of infinitely many frequencies ω . The strength of interaction is γ , and the bath spectral density is either Ohmic [$s = 1$ in Eq. (2)] or sub-Ohmic [$0 < s < 1$ in Eq. (2)], i.e., the modes are skewed towards lower frequencies in the latter case. The density matrix [Eq. (41)] of the two-level system is uniquely determined [17] by three real numbers of the Bloch vector \mathbf{P} , so that $|\mathbf{P}|$ quantifies purity of the spin or qubit mixed quantum state ($|\mathbf{P}(t=0)| = 1$ signifies pure state $\hat{\rho} = |\Sigma\rangle\langle\Sigma|$, while $|\mathbf{P}(t)| < 1$ indicates decoherence [18]). (b) Illustration of quantum spin chain with multiple bosonic baths [Eq. (3)]. The edge spins are coupled to vector baths kept at temperature T_1 or T_4 , i.e., the baths are composed of isotropic harmonic oscillators whose triple-degenerate modes couple to the corresponding component $\alpha = x, y, z$ of the spin operators located at the edge sites $n = 1$ and $n = 4$. Note that the spin-chain-boson model, aside from serving as a testbed for our calculations, is also of relevance to experiments in quantum spintronics [19–21] where such open quantum system is realized as a chain of magnetic atoms on a substrate which interact with a bosonic bath composed of phonons from the substrate [22, 23].

sipative and/or driven problems [32] in condensed matter and atomic-molecular-optical physics. However, it is applicable *only* to Markovian regime [15, 24–26, 32–34] requiring [7] that system-environment coupling is weak while environment correlations are short compared to the timescale of the system evolution. The Markovian limit ensures irreversible loss of characteristic quantum features, as well as that the future evolution of the system only depends on its present state and not on its history.

On the other hand, many applications, including notably quantum computers where a dissipative and noisy environment limits operational time of qubits [35, 36], involve open quantum systems exhibiting pronounced memory effects and thereby time-retarded dynamics. A hallmark of such non-Markovian regime is the revival of genuine quantum properties, such as quantum coherence, correlations, and entanglement [4, 5]. Such effects are enabled by non-Markovian backflow of information from the environment to the system. The ability to efficiently simulate non-Markovian open quantum systems also opens new avenues for optimal control [37] of open quantum systems, including via environmental engineering [38]. However, the non-Markovian open quantum systems exhibit exponential growth of complexity with the memory time of the environment, in quite analogous way to how complexity of closed quantum many-body systems grows with the number of degrees of freedom. This generally restricts many methods developed for non-Markovian regime to *very small system sizes*,

or if they can handle larger systems [39–43] they are typically restricted to short evolution times, choice of environment(s) [40, 41] and spatial geometry like one-dimensional (1D) chains [39, 42, 43] of systems each of which can interact with a single dissipative environment.

Thus, these unresolved challenges call for exploration of alternative avenues that could allow one to handle many mutually interacting quantum degrees of freedom, each of which is strongly coupled to possibly several structured environments. In addition, to describe experimentally relevant systems in quantum computing [35, 36, 44] or quantum spintronics [19–23] and quantum magnonics [45], one needs to handle arbitrary spatial dimensionality (including three-dimensional systems [44, 45]) and geometry [1] of both the degrees of freedom and their environments, and with ability to evolve for sufficiently long times of relevance to underlying physics.

In this study, we introduce a field-theoretic approach offering such capabilities. Our approach combines SKFT with a two-particle irreducible (2PI) effective action [27, 33, 46–48] that resums [49–52] classes of Feynman diagrams to infinite order. To reach *nonperturbative* regime in the system-environment coupling constant, as required [7, 40, 41] to handle non-Markovian dynamics, Feynman diagrams in our SKFT+2PI approach are obtained *not* from the expansion in the coupling constant, but by using $1/N$ expansion. Note that both $1/N$ expansion and 2PI resummation techniques were origi-

nally developed long ago for problems in high energy physics [29, 53, 54]. Nevertheless, it has only very recently been realized [55] why $1/N$ expansion can capture nonperturbative physics, namely, its terms can sometimes be fully decoded using resurgent transseries [52, 56] in the coupling constant.

To demonstrate the capabilities of our SKFT+2PI approach, we apply it to the spin-boson model [16] as an archetypical problem in the field of open quantum systems [2]. The spin-boson model, illustrated by Fig. 1(a), describes quantum spin $S = 1/2$ as two-level system interacting with an infinite bosonic bath as the dissipative environment. Despite its apparent simplicity [Eq. (1)], it contains plenty of challenges in the non-Markovian regime that have ignited development of numerous specialized approaches [57–72]. In fact, the spin-boson model is still often used [73–75] as a testbed when developing new approaches or refining the previous ones [76, 77]. Furthermore, we demonstrate that our SKFT+2PI approach can tackle a much more formidable problem of quantum spin chain interacting with many dissipative environments, as illustrated in Fig. 1(b). That is, its spins within XXX chain interact strongly with each other via antiferromagnetic exchange, while edge spins are additionally coupled to a set of three bosonic baths (one for each spin component) that are kept at two different temperatures. For both problems, we study dynamics of spin expectation values, as well as multitime two-spin correlators. We recall that even the exact knowledge of the evolution of the reduced density matrix from QME approaches [2, 8, 9, 78, 79] is *not sufficient* [39, 40] to obtain proper multitime correlations in the non-Markovian regime.

We carefully benchmark our SKFT+2PI calculations on the spin-boson model against: Lindblad QME in the Markovian regime; and in the non-Markovian regime, we use hierarchical equations of motion (HEOM) [79], as well as tensor network (TN) methods like time-evolving density operator with orthogonal polynomials algorithm (TEDOPA) [59, 64, 67], and time-evolving matrix product operator (TEMPO) [40, 63]. Our results in Figs. 4 and 5 demonstrate that SKFT+2PI can replicate results of all these four methods, while also being able to handle the spin-boson model at zero temperature (where HEOM breaks down), evolving over long times (at which both TEDOPA and TEMPO encounter problems at high temperature), and including a variety of bath spectral properties. Particular examples of SKFT+2PI results obtained for such challenging parameters within the non-Markovian regime are shown in Figs. 6 and 7. Furthermore, two-spin correlators are accessible with our SKFT+2PI approach, as exemplified by the delocalized-localized order parameter in the spin-boson model [Fig. 9], as well as computation of spin current in a spin-chain-boson [Fig. 10(e)]. Note that, in the case of spin-chain-boson we show only SKFT+2PI results in the non-Markovian regime as very few available recently developed methods [40, 41, 43] could not pro-

vide a proper benchmark due to complexity of the model chosen in Fig. 1(b) where each spin has three components and each component of edge spins is coupled to a different bath.

The paper is organized as follows. The spin-boson model and a plethora of previously developed approaches for its solution are overviewed in Sec. II A. In Sec. II C we construct the SKFT+2PI approach, which operates with Feynman diagrams generated by $1/N$ expansion, for open quantum systems. We provide details of TN, HEOM and Lindblad QME benchmark calculations in Secs. II D, II E and II F, respectively. We compare SKFT+2PI results to these benchmarks in Sec. III and Figs. 4, 5 and 6, while in Figs. 7, 8, and 9 we plot SKFT+2PI results only for the spin-boson model. In addition, Sec. III C shows SKFT+2PI treatment of open antiferromagnetic quantum spin chain. We conclude in Sec. IV.

II. MODELS AND METHODS

A. Spin-boson model

The spin-boson model [16] is a two-level quantum system—as realized by a spin $S = 1/2$, a qubit [35, 36], or any two well-separated energy levels [4, 5]—which is made open by its interaction with a bosonic bath composed of infinitely many harmonic oscillators [16]. We illustrate this model in Fig. 1(a). Although it has been intensely studied for nearly four decades [16], its non-Markovian dynamics [4, 10, 67, 80, 81] still pose a formidable challenge despite the plethora of available numerical and analytical methods [57–73, 76, 77] for open quantum systems developed specifically for it. This is especially true for the case of zero [61, 73, 81] or ultralow temperatures and/or specific frequency content of the bosonic bath [61, 80]. Such limit is of particular relevance to superconducting qubits [35, 36, 44] subjected to electromagnetic noise [70], which can be modeled by non-Markovian dynamics of a spin interacting with a sub-Ohmic bath at ultralow temperature. The zero or ultralow temperature makes strong quantum effects and long memory time of the bath pronounced, while transition from coherent damped motion to localization is generated by increasing the system-bath coupling strength [60].

The Hamiltonian of the total spin+bath system is given by

$$\hat{H} = \frac{\omega_q}{2} \hat{\sigma}^z + \frac{\Delta}{2} \hat{\sigma}^x + \sum_k \omega_k \hat{b}_k^\dagger \hat{b}_k + \hat{\sigma}^z \sum_k \frac{g_k}{2} (\hat{b}_k + \hat{b}_k^\dagger), \quad (1)$$

where $\hbar = 1$ for simplicity of notation; $\hat{\sigma} = (\hat{\sigma}^x, \hat{\sigma}^y, \hat{\sigma}^z)$ is the vector of the Pauli operators; ω_q is the energy difference between the two eigenstates of $\hat{\sigma}^z$, $\hat{\sigma}^z |\uparrow\rangle = |\uparrow\rangle$, $\hat{\sigma}^z |\downarrow\rangle = -|\downarrow\rangle$; Δ is the tunneling matrix element, which also sets the units of energy; \hat{b}_k^\dagger and \hat{b}_k are bosonic creation and annihilation operators, respectively;

and the spin is coupled with strength g_k to the k -th mode of the bath via the fourth term on the right-hand side (RHS) of Eq. (1). The impact of the bath on the spin is fully captured by the coupling-weighted spectral density, $\mathcal{J}(\omega) = 2\pi \sum_k g_k^2 \delta(\omega - \omega_k)$, for which a generic form

$$\mathcal{J}(\omega) = \gamma \omega_c^{1-s} \omega^s e^{-\omega/\omega_c}, \quad (2)$$

is usually assumed [16]. Here γ is the parameter characterizing system-bath coupling strength; ω_c is the characteristic or cutoff frequency of the bath; parameter $0 < s < 1$, $s = 1$ and $s > 1$ classifies spectral densities as sub-Ohmic, Ohmic and super-Ohmic, respectively [61]; and the spectral density $\mathcal{J}(-\omega) = -\mathcal{J}(\omega)$ is antisymmetrically extended [57]. We illustrate the spectral content of different bosonic baths in Fig. 1(a). The sub-Ohmic case, with a relatively large portion of low-frequency modes, is considered particularly challenging [61, 68–71, 76] at zero temperature ($k_B T = 0$). Other challenges are, in general, posed by the long-time limit [61, 76, 77, 82] of non-Markovian dynamics [80, 81], whose memory effects force information to flow from the environment back to the system and such effects are not necessarily transient [80]. It is generically assumed that non-Markovian regime [4, 10, 67] in open quantum system dynamics is entered when the system-bath coupling is sufficiently strong and correlations of the bath do not decay rapidly [7]. But detailed examination [80, 81] of measures of non-Markovianity vs. system-bath coupling strength in the case of spin-boson model shows complex nonmonotonic dependence, including sensitivity to the cutoff frequency ω_c . In the non-Markovian regime, one finds recoherence effects and a departure from purely exponential decay in the dynamics of system observables. This is also illustrated by comparing our results for Markovian vs. non-Markovian dynamics in Figs. 4 vs. 5 and 6, respectively.

The brute force numerical solution of QME in the non-Markovian regime requires computing high-dimensional integrals over time [78], where accuracy of calculations become extremely sensitive to numerical errors. As an alternative, the widely-used HEOM approach [79] has been developed by converting time-nonlocal integro-differential QME of the brute force method [78] into a set of finitely many time-local differential equations. However, its standard version [79] is limited to high temperatures [83], which has motivated recent efforts to extend HEOM approach [76, 77, 82] to access zero temperature and much longer simulation times. Multilayer multiconfiguration time-dependent Hartree (ML-MCTDH) [60, 61], numerical renormalization group (NRG) [68–71], self-consistent dynamical maps [74] and TN approaches that can handle non-Markovian dynamics at zero temperature have also been developed. However, HEOM and ML-MCTDH algorithms are prohibitively expensive for many interacting quantum spins or, equivalently, qubits [35, 36].

The TN approaches to non-Markovian dynamics of open quantum systems broadly divide into two comple-

mentary classes [75]. One class, which hosts TEDOPA used in our study as a benchmark [Figs. 4, 5, and 6], is based on applying a thermofield chain mapping [59, 67]. This approach purifies a finite temperature environment and transforms its representation into a chain geometry ideally suited to matrix product state (MPS) algorithms. Then, the pure quantum state of the full system and environment is unitarily evolved using well established MPS techniques like the time-dependent variational principle (TDVP) [84, 85]. The other class is, instead, based on applying a matrix product operator (MPO) to describe the Feynman-Vernon influence functional in the temporal domain [40, 63, 64, 73, 86, 87], or, more generally, a process tensor (PT) [39–41, 65, 88, 89]. TEMPO, the second TN-based benchmark we also employ [Figs. 4, 5, and 6], belongs to this class. The strongest limitation of TEDOPA is short time evolution. Although TN-based approaches can handle many interacting quantum spins, they are also prohibitively expensive in higher dimensions or when time evolution exhibits a transient “entanglement barrier” [90–92]. For example, even Markovian dynamics can lead to a spike [93] of the many-body entanglement of the system, despite the presence of a dissipative environment and naïve expectation [94] that interactions with the environment should curtail entanglement growth. Moreover, the chain mapping representation of an environment spectral function is also truncated to a finite length which limits the time the simulation can reach while faithfully capturing the environment’s continuum [95, 96]. For TEMPO and PT-TEMPO there is a combination of Trotter errors and truncation errors from the compression of the MPS bond dimension whose interplay is not currently fully understood and alas limits the reachable simulation times [86, 87].

Thus, the need for new approaches for non-Markovian dynamics of many locally interacting quantum spins surrounded by dissipative environment motivates development of SKFT+2PI theory in Sec. II C with its diagrammatic expansion formulated in terms of Keldysh (or nonequilibrium) Green’s functions (GFs).

B. Spin-chain-boson model

To make the discussion transparent, we formulate SKFT approach by starting from a specific Hamiltonian

$$\hat{H} = \frac{\mathbf{h}}{2} \cdot \sum_{n=1}^{N_S} \hat{\boldsymbol{\sigma}}_n + \frac{1}{4} \sum_{nn'} J_{nn'}^{\alpha\beta} \hat{\sigma}_n^\alpha \hat{\sigma}_{n'}^\beta + \sum_{nk} \omega_{nk} \hat{\mathbf{b}}_{nk}^\dagger \hat{\mathbf{b}}_{nk} + \frac{1}{2} \sum_{n\alpha k} g_{nk}^\alpha \hat{\sigma}_n^\alpha (\hat{b}_{nk}^{\alpha\dagger} + \hat{b}_{nk}^\alpha), \quad (3)$$

which is more general than Eq. (1) as it describes *many* spins mutually interacting via the Heisenberg exchange $J_{nn'}^{\alpha\beta}$ between the $\alpha, \beta = x, y, z$ components of spins at sites n and n' . The spin at site n is itself an open quantum system, as its Cartesian components couple to

three bosonic baths, i.e., one bath for each spin component. The frequencies ω_{nk} are the same for all three baths at site n and obey a spectral density given by Eq. (2). Baths at different sites are independent, and $\hat{\mathbf{b}}_{nk} = (\hat{b}_{nk}^x, \hat{b}_{nk}^y, \hat{b}_{nk}^z)^T$ are the canonical bosonic operators of the bath. The spin-boson Hamiltonian of Eq. (1) is obviously a special case of our general Hamiltonian in Eq. (3) in which the number of spins is $N_S = 1$; the external magnetic field is $\mathbf{h} = (\Delta, 0, \omega_q)$; $J_{11}^{\alpha\beta} = 0$; and g_{1k}^z are the only nonzero spin-bath couplings.

C. Schwinger-Keldysh field theory + 2PI for both Markovian and non-Markovian dynamics

Defining the functional integral of SKFT for the Hamiltonian in Eq. (3) is cumbersome due to spin operator commutation relations [48]. Instead, it is more convenient to map the spin operators in the Hamiltonian of Eq. (3) onto fermionic or bosonic operators [97] subject to canonical commutation relations, so that the Wick theorem and other field-theoretic machinery applicable to such operators can be utilized. Here we employ the Schwinger boson mapping [48, 98, 99], in which operators of spin S are expressed as

$$\hat{\sigma}_n^\alpha = \hat{\psi}_n^\dagger \boldsymbol{\sigma}^\alpha \hat{\psi}_n, \quad (4)$$

where $\boldsymbol{\sigma}^\alpha$ is a matrix representation of the Pauli operators, and $\hat{\psi}_n = (\hat{a}_n^1, \hat{a}_n^2)^T$ is a doublet of the two Schwinger bosons for spin n . The number of bosons is constrained to be

$$\hat{a}_n^{(1)\dagger} \hat{a}_n^{(1)} + \hat{a}_n^{(2)\dagger} \hat{a}_n^{(2)} = 2S, \quad (5)$$

for each spin S . The constraint ensures that only a subspace of the infinite dimensional bosonic Hilbert space is utilized for spin dynamics, such as $|1, 0\rangle \equiv |\uparrow\rangle$, $|0, 1\rangle \equiv |\downarrow\rangle$ spanning the physical Hilbert space in the case of spin $S = 1/2$. Unlike imaginary time applications of Schwinger bosons which require explicitly introducing the constraint in Eq. 5 via Lagrange multipliers [98, 99], the conserved currents associated with the symmetries of the Schwinger-Keldysh action automatically enforce this constraint throughout the real time evolution [48]. Although other mappings from spin to bosons or fermions can be employed, Schwinger bosons preserve rotational symmetry, as opposed to Holstein-Primakoff bosons [100]; and are also generalizable to larger spin value S , unlike Majorana [47] or Jordan-Wigner [101] fermions applicable only to $S = 1/2$.

The Schwinger-Keldysh functional integral is formulated in terms of complex fields ψ_n which are eigenvalues

$$\hat{\psi}_n |\psi_1, \dots, \psi_n, \dots, \psi_{N_S}\rangle = \psi_n |\psi_1, \dots, \psi_n, \dots, \psi_{N_S}\rangle, \quad (6)$$

of $\hat{\psi}_n$ and the corresponding eigenvectors $|\psi_1, \dots, \psi_n, \dots, \psi_{N_S}\rangle$ are the bosonic coherent states.

The real fields of the position and momentum representation, $a_n^\sigma = (x_n^\sigma + ip_n^\sigma)/\sqrt{2}$, are grouped into the 4-component field

$$\varphi_n = (x_n^{(1)}, p_n^{(1)}, x_n^{(2)}, p_n^{(2)})^T. \quad (7)$$

The spin fields can be constructed as $\sigma_n^\alpha = \varphi_n^T K^\alpha \varphi_n / 2$, where

$$K^x = \boldsymbol{\sigma}^x \otimes I_2, \quad K^y = -\boldsymbol{\sigma}^y \otimes \boldsymbol{\sigma}^y, \quad K^z = \boldsymbol{\sigma}^z \otimes I_2, \quad (8)$$

and I_2 is the 2×2 identity matrix. Then, the Schwinger-Keldysh action, $S = S_S + S_B$, one of the central quantities in SKFT, is obtained as

$$S_S = - \int_{\mathcal{C}} dt \sum_n \varphi_n^T \left(\frac{i}{2} K^0 \partial_t + H \right) \varphi_n + \sum_{\alpha\beta nn'} J_{nn'}^{\alpha\beta} \sigma_n^\alpha \sigma_{n'}^\beta, \quad (9a)$$

$$S_B = \int_{\mathcal{C}} dt \sum_{n\alpha k} [b_{nk}^{\alpha*} (i\partial_t - \omega_{nk}) b_{nk}^\alpha - g_{nk}^\alpha \sigma_n^\alpha (b_{nk}^\alpha + b_{nk}^{\alpha*})], \quad (9b)$$

by time evolving the Lagrangian corresponding to the general Hamiltonian in Eq. (3) along the Schwinger-Keldysh closed time contour \mathcal{C} [26–29]. Here S_S and S_B are the contributions to the total action S from the system of spins and the bath, respectively; $K^0 = I_2 \otimes \boldsymbol{\sigma}^y$; and

$$H = \sum_\alpha h^\alpha K^\alpha / 4. \quad (10)$$

The action of the bath is in the Gaussian form, so it can be integrated out exactly. This leaves behind a quartic term

$$\propto \sigma_n^\alpha(t) \Xi_n^\alpha(t, t') \sigma_n^\alpha(t') \quad (11)$$

in the total action, representing a *nonlocal-in-time* effective self-interaction of the spin generated by the presence of the bath. The bath kernel

$$\Xi_n^\alpha(t, t') = \sum_k (g_{nk}^\alpha)^2 B_{nk}^\alpha(t - t'), \quad (12)$$

is given in terms of the Keldysh GF of the bosonic bath

$$iB_{nk}^\alpha(t - t') = \langle b_{nk}^\alpha(t) b_{nk}^{\alpha*}(t') \rangle, \quad (13)$$

which consists of four components [26, 29, 102, 103] because of four possibilities for placing two times t and t' on the forward and backward branches of the Schwinger-Keldysh contour \mathcal{C} . Here, $\langle \dots \rangle$ is the nonequilibrium expectation value (EV) [26]. The temperature of the bath $k_B T$ is a parameter within the components of the bath kernel Ξ_n^α . The quartic terms, one from Eq. (11) and the other one from the Heisenberg interaction in the Hamiltonian of Eq. (3), can be decoupled through Hubbard-Stratonovich transformations [104], yielding the modified

total action

$$S = \int_C dt \left[- \sum_n \varphi_n^T \left(\frac{i}{2} K^0 \partial_t + \tilde{H}_n \right) \varphi_n \right. \\ \left. + \frac{1}{4} \int_C dt' \sum_{\alpha n} \frac{\lambda_n^\alpha(t) \lambda_n^\alpha(t')}{\Xi_n^\alpha(t, t')} + \frac{1}{4} \sum \Lambda_n^\alpha [J^{-1}]_{nn'}^{\alpha\beta} \Lambda_{n'}^\beta \right], \quad (14)$$

where λ_n^α and Λ_n^α are the Hubbard-Stratonovich fields that mediate the bath-induced nonlocal-in-time interaction and the Heisenberg interaction, respectively, and $\tilde{H}_n = H + \frac{1}{4} \sum_\alpha (\lambda_n^\alpha + \Lambda_n^\alpha) K^\alpha$ is the effective magnetic field. Note that Λ_n^α can be interpreted as the α -component of the magnetic mean-field acting by which other spins act on the spin at site n .

To progress from the modified total action in Eq. (14), several routes are possible. For instance, the *quantum* (for the bath)-*classical* (for spins) regime can be probed by minimizing the action with respect to quantum fluctuations which emerge naturally in the SKFT formalism due to the Schwinger-Keldysh closed time contour. This then leads to integro-differential equations, rigorously deriving and extending otherwise phenomenological Landau-Lifshitz equation, that contain a time-retarded (i.e., non-Markovian) dissipation kernel accounting for the bath [25, 105–107]. The form of these equations [108, 109] is quite analogous to the Nakajima-Zwanzig equation [8, 9]. The time-retarded kernel can be either approximated by analytical means [105, 107], or solved numerically [106]. In the quantum-classical regime, the memory of the bath is encoded in the dissipation kernel, which is a feature completely missed in SKFT approaches to open quantum systems where Markovianity is built into the Schwinger-Keldysh functional integral [24, 25, 110].

Alternatively, the fully quantum regime of the modified total action in Eq. (14) can be captured by deriving the Dyson equations for the n -particle correlation functions [26, 29]. However, an additional scheme is required in order to handle the self-consistent nature of the ensuing self-energy (SE) and approximate it in a controllable manner. Here, we borrow from elementary particle physics [29] the 2PI effective action formalism [27, 111] which sums [49] an infinite number of Feynman diagrams of particular topology [54] where the coupling constant in the diagrammatic expansion is $1/N$ [47, 48, 112–116], with N being the number of Schwinger bosons employed to map the spin operators in the Hamiltonian of Eq. (3). This can unravel effects that are *nonperturbative* [54, 55] in the system-bath couplings γ_n^α , which would otherwise be unattainable when using standard perturbative expansion [103, 117, 118] in the couplings γ_n^α . For example, our results for the spin-boson model in Fig. 5 follow remarkably closely what are considered numerically exact benchmarks, as obtained from HEOM, TEDOPA, and TEMPO calculations, despite considering only a subset of all possible Feynman diagrams. Interestingly, the number $N = 2$ of Schwinger bosons we employ, despite

not being as large as usually invoked in $1/N$ expansions used in elementary particle physics [54], is sufficient to produce accurate results [113].

The 2PI effective action is obtained from the connected generating functional

$$W[J, K] = -i \ln \int \mathcal{D}\Phi \exp \left(iS[\Phi] + i \int_C dt J(t) \Phi(t) \right. \\ \left. + \int_C dt dt' K(t, t') \Phi(t) \Phi(t') \right), \quad (15)$$

where $\mathcal{D}\Phi$ indicates functional integration over all possible configurations of six-component field $\Phi = (\varphi, \lambda, \Lambda)^T$, and J and K are one- and two-particle sources [29, 48], respectively. The Legendre transform of the functional $W[J, K]$ with respect to both arguments is the 2PI effective action

$$\Gamma[\bar{\Phi}, G] = W[J, K] - \int_C dt J(t) \bar{\Phi}(t) \\ - \frac{1}{2} \int_C dt dt' K(t, t') \left(G(t', t) - i \bar{\Phi}(t') \bar{\Phi}(t) \right). \quad (16)$$

Here, $\bar{\Phi}$ and G are the one- and two-particle connected EVs generated by $W[J, K]$. That is, $\bar{\Phi}$ is the EV of the fields and G is the connected Keldysh GF. Although both $W[J, K]$ and $\Gamma[\bar{\Phi}, G]$ hold the same information, the former produces EVs via functional derivatives in the limit of vanishing sources, whereas the latter produces them through a comparatively simpler variational approach, that is, the EVs satisfy $\delta\Gamma/\delta\bar{\Phi} = 0$ and $\delta\Gamma/\delta G = 0$. Such variational calculations can be performed on the expansion [53]

$$\Gamma[\bar{\Phi}, G] = S[\bar{\Phi}] + \frac{i}{2} \text{Tr} \ln G^{-1} + \frac{i}{2} \text{Tr} [G_0^{-1} [\bar{\Phi}] G] - i\Gamma_2, \quad (17)$$

where a constant term has been ignored; the trace is taken over all possible indices and times; $G_0^{-1} = \delta^2 S / \delta \bar{\Phi} \delta \bar{\Phi}$ is the inverse of the free Keldysh GF (i.e., ignoring terms cubic and higher-order in the fields); and Γ_2 contains all the 2PI vacuum diagrams. These 2PI vacuum diagrams are those that cannot be separated by cutting two edges or fewer. Edges represent Keldysh GF G and vertices correspond to interactions contained in the action S .

The spin-to-Schwinger-boson mapping implies that any EV containing an odd number of Schwinger bosons vanishes for physical states. In particular, $\bar{\varphi} = 0$ and $\langle \varphi(t) \lambda(t') \rangle = \langle \varphi(t) \Lambda(t') \rangle = 0$. Additionally, the absence of terms in the action of Eq. (14) that couple λ_n^α and Λ_n^α means that $\langle \lambda_n^\alpha(t) \Lambda_{n'}^\beta(t') \rangle = 0$. The remaining non-vanishing EVs are summarized in Table I. Taking this into account, the equations of motion for the EVs of the fields and the connected Keldysh GFs obtained from the expansion of the 2PI action in Eq. (17) via variational principle are given by

Symbol	Definition	Name	Symbol	Definition	Name
$\Xi_n^\alpha(t, t')$	$\sum_k (g_{nk}^\alpha)^2 B_{nk}^\alpha(t - t')$	Bath kernel	$\bar{\lambda}_n^\alpha(t)$	$\langle \lambda_n^\alpha(t) \rangle$	EV of the bath field
$J_{nn'}^{\alpha\beta}$		Heisenberg coupling	$\bar{\Lambda}_n^\alpha(t)$	$\langle \Lambda_n^\alpha(t) \rangle$	EV of the mean-field
$g_n^{ab}(t, t')$	$-i \langle \varphi_n^b(t') \varphi_n^a(t) \rangle$	GF of the Schwinger bosons	$\Sigma_n^{ab}(t, t')$	$2\delta\Gamma_2/\delta g$	SE of the Schwinger bosons
$D_n^\alpha(t, t')$	$-i \langle \lambda_n^\alpha(t') \lambda_n^\alpha(t) \rangle + i \bar{\lambda}_n^\alpha(t) \bar{\lambda}_n^\beta(t')$	Bath propagator	$\Pi_n^\alpha(t, t')$	$2\delta\Gamma_2/\delta D$	SE of the bath
$M_{nn'}^{\alpha\beta}(t, t')$	$-i \langle \Lambda_{n'}^\alpha(t') \Lambda_n^\beta(t) \rangle + i \bar{\Lambda}_n^\alpha(t) \bar{\Lambda}_{n'}^\beta(t')$	Mean-field propagator	$\Omega_n^{\alpha\beta}$	$2\delta\Gamma_2/\delta M$	SE of the mean-field
$\tilde{M}_{nn'}^{\alpha\beta}(t, t')$	Eq. (25)	Mean-field propagator			
\tilde{H}_n^{ab}	$H^{ab} + \frac{1}{4} \sum_\alpha (\lambda_n^\alpha + \Lambda_n^\alpha) K_{ab}^\alpha$	Effective Hamiltonian	K_{ab}^α	Eq. (8)	Spin matrices for real fields

TABLE I. Summary of the key quantities of our SKFT+2PI framework for open quantum spin systems which appear in the equations of motion, Eqs. (18) and (26), with their respective symbols, definitions, and labels. All indices are shown explicitly, such as $a, b = 1 \dots 4$, $\alpha, \beta = x, y, z$, and $n = 1 \dots N_S$.

$$\bar{\lambda}_n^\alpha(t) = \frac{i}{2} \int_{\mathcal{C}} dt' \Xi_n^\alpha(t, t') \text{Tr}_S[K^\alpha g_n(t', t)], \quad (18a)$$

$$\bar{\Lambda}(t) = \frac{i}{2} J \text{Tr}_S[Kg(t, t)], \quad (18b)$$

$$D_n^\alpha(t, t') = 2\Xi_n^\alpha(t, t') + 2 \int_{\mathcal{C}} dt_1 dt_2 \Xi_n^\alpha(t, t_1) \Pi_n^\alpha(t_1, t_2) D_n^\alpha(t_2, t'), \quad (18c)$$

$$M(t, t') = 2J\delta_{tt'} + 2 \int_{\mathcal{C}} dt_1 J\Omega(t, t_1) M(t_1, t'), \quad (18d)$$

$$\partial_t g_n(t, t') = iK^0 \delta_{tt'} + 2iK^0 \tilde{H}_n(t) g_n(t, t') + iK^0 \int_{\mathcal{C}} dt_1 \Sigma_n(t, t_1) g_n(t_1, t'). \quad (18e)$$

Note that all integrals $\int_{\mathcal{C}}$ are over the Schwinger-Keldysh closed contour. Here, matrix multiplication is assumed for indices not shown (see Table I); Tr_S traces over the space of Schwinger boson; $\delta_{tt'}$ is the contour Dirac delta function [27]; and $\Pi = 2\delta\Gamma_2/\delta D$, $\Omega = 2\delta\Gamma_2/\delta M$, and $\Sigma = 2\delta\Gamma_2/\delta g$ are the SEs derived through functional differentiation of the 2PI vacuum diagrams. Although the GF of the Schwinger bosons $g_{nn'}$ can in principle be non-local, constraints of the initial state imply $g_{nn'} = g_n \delta_{nn'}$. Equations (18) do not form a closed system due to the infinite diagrammatic summation within the SE terms, so a *controlled approximation* scheme is required.

One possibility is to neglect Γ_2 in Eq. (17), which leads to classical dynamics of spin of the Landau-Lifshitz type [105–107]. For fully quantum dynamics of spin, the diagrammatic expansion of Γ_2 needs to be truncated. We adopt the scheme used in Ref. [48], where diagrams are truncated based on powers of the inverse of the number of Schwinger bosons $1/N$, which has been previously shown to adequately capture the relevant features of closed quantum systems [48, 114]. Each diagram in

the expansion is made up of vertices

$$\begin{array}{c} \varphi_n \\ \diagup \\ \text{---} \lambda_n^\alpha \text{---} K^\alpha \\ \diagdown \\ \varphi_n \end{array} = -\frac{i}{4} K_{ab}^\alpha \varphi_n^a(t) \varphi_n^b(t) \lambda_n^\alpha(t), \quad (19)$$

$$\begin{array}{c} \varphi_n \\ \diagup \\ \text{---} \Lambda_n^\alpha \text{---} K^\alpha \\ \diagdown \\ \varphi_n \end{array} = -\frac{i}{4} K_{ab}^\alpha \varphi_n^a(t) \varphi_n^b(t) \Lambda_n^\alpha(t), \quad (20)$$

where outgoing solid lines correspond to a Schwinger boson field φ_n and dashed (curly) lines to the bath field λ_n^α (mean-field Λ_n^α). Within a particular diagram, closed loops of solid lines scale proportional to the number of Schwinger bosons $\mathcal{O}(N)$ due to being traced over this space, while dashed lines scale as $\mathcal{O}(1/N)$. This can be inferred from the action in Eq. (14), where $\Xi \sim \mathcal{O}(1/N)$, and the equation of motion for D [Eq. (18c)] because $D \sim \Xi$. A similar argument can be used to determine that curly lines also scale as $\mathcal{O}(1/N)$. Thus, the 2PI diagrams with the lowest scaling are the two-loop ones:

$$\Gamma_2 = \text{---} \bigcirc \text{---} + \text{---} \bigcirc \text{---} \sim \mathcal{O}(1). \quad (21)$$

At this order of truncation, the corresponding SEs are

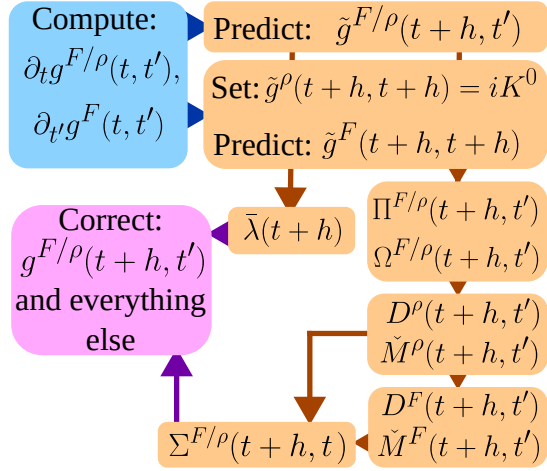


FIG. 2. The flow chart of the predictor-corrector method used to solve system of Eqs. (26). Due to the symmetries of the statistical F and spectral ρ components of double-time Keldysh GFs, it suffices to compute them only for times $t' \leq t$.

given by

$$\Pi_n^\alpha(t, t') = \frac{i}{8} \text{Tr}_S[K^\alpha g_n(t, t') K^\alpha g_n^T(t, t')], \quad (22a)$$

$$\Omega_n^{\alpha\beta}(t, t') = \frac{i}{8} \text{Tr}_S[K^\alpha g_n(t, t') K^\beta g_n^T(t, t')], \quad (22b)$$

$$\begin{aligned} \Sigma^{ab}(t, t') &= \frac{i}{4} \sum_\alpha K^\alpha g_n(t, t') K^\alpha D_n^\alpha(t, t') \\ &+ \frac{i}{4} \sum_{\alpha\beta} K^\alpha g_n(t, t') K^\beta M_{nn}^{\alpha\beta}(t, t'). \end{aligned} \quad (22c)$$

Note that all the lines of 2PI diagrams in Eq. (21) are fully interacting, or dressed, Keldysh GFs which already contain an infinite series of diagrams in terms of the noninteracting, or free, Keldysh GFs. The self-consistency [49] built into 2PI resummation evades [46]

the so-called secularity problem for expansion in terms of the free Keldysh GFs, where elapsed time appearing next to the coupling constant makes the effective coupling arbitrarily large at late times. The same self-consistency ensures that all global conservation laws are satisfied [102].

Equations (18) and (22) are defined on the Schwinger-Keldysh closed time contour and are, therefore, complex. The real time equations are obtained by decomposing the contour GFs [27] as

$$G(t, t') = G^F(t, t') + \frac{1}{2} \text{sgn}_C(t, t') G^\rho(t, t'). \quad (23)$$

The statistical and spectral

$$G^F = \frac{1}{2}(G^> + G^<), \quad G^\rho = G^> - G^<, \quad (24)$$

parts of the Keldysh GFs, respectively, are in turn related to the lesser and greater GFs, commonly employed in operator formulation of Keldysh GFs [102, 103]. The arguments of G^F and G^ρ take values in real time, while the sign function $\text{sgn}_C(t, t')$ equals 1 if its arguments are ordered on the contour or -1 vice versa. Through this decomposition, integrals over \mathcal{C} simplify to real time integrals (which in operator language requires usage of the much more demanding Langreth rules [102, 119]) that preserve causality. The decomposition of $M_{nn'}^{\alpha\beta}(t, t')$ requires special care due to having a time-local part proportional to $\delta_{tt'}$. The time-local part can be extracted by defining $\check{M}_{nn'}^{\alpha\beta}(t, t')$ such that

$$M(t, t') = 2J\delta_{tt'} + J\check{M}(t, t')J. \quad (25)$$

Assuming that there is no single-ion anisotropy, i.e., $J_{nn}^{\alpha\beta} = 0$, no other GFs or SEs have a time-local component. Therefore, these decompositions yield the real-time equations of motion

$$\partial_t g_n^F(t, t') = 2iK^0 \tilde{H}_n(t) g_n^F(t, t') + iK^0 \int_0^t dt_1 \Sigma_n^\rho(t, t_1) g_n^F(t_1, t') - iK^0 \int_0^{t'} dt_1 \Sigma_n^F(t, t_1) g_n^\rho(t_1, t'), \quad (26a)$$

$$\partial_t g_n^\rho(t, t') = 2iK^0 \tilde{H}_n(t) g_n^\rho(t, t') + iK^0 \int_{t'}^t dt_1 \Sigma_n^\rho(t, t_1) g_n^\rho(t_1, t'), \quad (26b)$$

$$\begin{aligned} D_n^{\alpha F}(t, t') &= 2\Xi_n^{\alpha F}(t, t') + 2 \int_0^t \int_0^{t_1} dt_1 dt_2 \Xi_n^{\alpha\rho}(t, t_1) \Pi_n^{\alpha\rho}(t_1, t_2) D_n^{\alpha F}(t_2, t') \\ &+ 2 \int_0^{t'} \int_0^{t_1} dt_1 dt_2 \Xi_n^{\alpha F}(t, t_2) \Pi_n^{\alpha\rho}(t_2, t_1) D_n^{\alpha\rho}(t_1, t') - 2 \int_0^t \int_0^{t'} dt_1 dt_2 \Xi_n^{\alpha\rho}(t, t_1) \Pi_n^{\alpha F}(t_1, t_2) D_n^{\alpha\rho}(t_2, t'), \end{aligned} \quad (26c)$$

$$D_n^{\alpha\rho}(t, t') = 2\Xi_n^{\alpha\rho}(t, t') + 2 \int_{t'}^t \int_{t'}^{t_1} dt_1 dt_2 \Xi_n^{\alpha\rho}(t, t_1) \Pi_n^{\alpha\rho}(t_1, t_2) D_n^{\alpha\rho}(t_2, t'), \quad (26d)$$

$$\check{M}^F(t, t') = 4\Omega^F(t, t') + 2 \int_0^t dt_1 \Omega^\rho(t, t_1) J\check{M}_n^F(t_1, t') - 2 \int_0^{t'} dt_1 \Omega^F(t, t_1) J\check{M}^\rho(t_1, t') \quad (26e)$$

$$\check{M}^\rho(t, t') = 4\Omega^\rho(t, t') + 2 \int_{t'}^t dt_1 \Omega^\rho(t, t_1) J \check{M}_n^\rho(t_1, t') - 2 \int_0^{t'} dt_1 \Omega^F(t, t_1) J \check{M}^\rho(t_1, t') \quad (26f)$$

$$\begin{aligned} \Sigma_n^F(t, t') &= \frac{i}{4} \sum_\alpha \left\{ K^\alpha g_n^F(t, t') K^\alpha D_n^{\alpha F}(t, t') + \frac{1}{4} K^\alpha g_n^\rho(t, t') K^\alpha D_n^{\alpha \rho}(t, t') \right\} \\ &+ \frac{i}{4} \sum_{\alpha\beta} \left\{ K^\alpha g_n^F(t, t') K^\beta [J \check{M}^F(t, t') J]_{nn}^{\alpha\beta} + \frac{1}{4} K^\alpha g_n^\rho(t, t') K^\beta [J \check{M}^\rho(t, t') J]_{nn}^{\alpha\beta} \right\}, \end{aligned} \quad (26g)$$

$$\begin{aligned} \Sigma_n^\rho(t, t') &= \frac{i}{4} \sum_\alpha \left\{ K^\alpha g_n^F(t, t') K^\alpha D_n^{\alpha \rho}(t, t') + K^\alpha g_n^\rho(t, t') K^\alpha D_n^{\alpha F}(t, t') \right\} \\ &+ \frac{i}{4} \sum_{\alpha\beta} \left\{ K^\alpha g_n^F(t, t') K^\beta [J \check{M}^\rho(t, t') J]_{nn}^{\alpha\beta} + K^\alpha g_n^\rho(t, t') K^\beta [J \check{M}^F(t, t') J]_{nn}^{\alpha\beta} \right\}, \end{aligned} \quad (26h)$$

$$\Pi_n^{\alpha F}(t, t') = \frac{i}{8} \text{Tr}_S [K^\alpha g_n^F(t, t') K^\alpha g_n^{F T}(t, t')] + \frac{i}{32} \text{Tr}_S [K^\alpha g_n^\rho(t, t') K^\alpha g_n^{\rho T}(t, t')], \quad (26i)$$

$$\Pi_n^{\alpha \rho}(t, t') = \frac{i}{4} \text{Tr}_S [K^\alpha g_n^F(t, t') K^\alpha g_n^{\rho T}(t, t')], \quad (26j)$$

$$\Omega_n^{\alpha \beta F}(t, t') = \frac{i}{8} \text{Tr}_S [K^\alpha g_n^F(t, t') K^\beta g_n^{F T}(t, t')] + \frac{i}{32} \text{Tr}_S [K^\alpha g_n^\rho(t, t') K^\beta g_n^{\rho T}(t, t')], \quad (26k)$$

$$\Omega_n^{\alpha \beta \rho}(t, t') = \frac{i}{4} \text{Tr}_S [K^\alpha g_n^F(t, t') K^\beta g_n^{\rho T}(t, t')], \quad (26l)$$

$$\bar{\lambda}_n^\alpha(t) = \frac{i}{2} \int_0^t dt_1 \Xi_n^{\alpha \rho}(t, t_1) \text{Tr}_S [K^\alpha g_n^F(t_1, t_1)], \quad (26m)$$

$$\bar{\Lambda}_n^\alpha(t) = \frac{i}{2} \sum_{\beta n'} J_{nn'}^{\alpha \beta} \text{Tr}_S [K^\beta g_{n'}^F(t_1, t_1)]. \quad (26n)$$

These equations form an integro-differential system of the Volterra type [120] that must be integrated carefully due to the self-consistent interdependence between 14 functions. For this purpose, we discretize both time arguments t and t' , and we employ a predictor-corrector algorithm [see Fig. 2 for a flow chart describing the numerical implementation]. Note that all functions satisfy

$$O^{F, \rho}(t, t') = \pm O^{F, \rho T}(t', t), \quad (27)$$

so that calculations at times $t' \leq t$ are sufficient. We first compute the RHS of Eqs. (26a) and (26b) by plugging in the functions at the current time step t and t' . Then, we predict the functions at the next time step $t+h$ as, e.g., $\tilde{g}_n^F(t+h, t') = g_n^F(t, t') + h \partial_t g_n^F(t, t')$. Predicting the diagonal time step, i.e., $\tilde{g}_n^F(t+h, t+h)$, requires the derivative with respect to the second time argument, $\partial_{t'} g_n^F(t, t')$, obtained from the transpose of Eq. (26a) and the symmetry properties of the Keldysh GFs. The time-diagonal of $g_n^\rho(t, t) = -i[\langle \varphi_n^b(t), \varphi_n^a(t) \rangle]$ is fixed by the equal-time commutation relations of the real Schwinger bosons, so we set it to $g_n^\rho(t, t) = iK^0$. All integrals are discretized using the trapezoid method and identical time increment h . Predictions for all subsequent functions are obtained in the order shown in Fig. 2, starting with plugging $\tilde{g}_n^F(t+h, t')$, $\tilde{g}_n^\rho(t+h, t')$ into Eqs. (26i)–(26l). The predictions for all functions are then used to recompute the RHS of Eqs. (26a) and (26b) to get $g_n^F(t+h, t') = g_n^F(t, t') + \frac{h}{2} [\partial_t g_n^F(t, t') + \partial_t \tilde{g}_n^F(t+h, t')]$. Additional de-

tails of this type of predictor-corrector scheme can be found in Ref. [48].

The SKFT+2PI approach allows for initial density matrix that is Gaussian [27, 47, 48], i.e., the only nonzero EVs at the initial time are that of single fields or product of two fields. For spin systems without fractional excitations [99, 121], correlations between Schwinger bosons at different sites vanish, $g_{nn'}^{ab} = g_n^{ab} \delta_{nn'}$, implying that $\Sigma_{nn'} = \Sigma_n \delta_{nn'}$ and similarly for the other SEs. This means that at time $t = 0$, we need to use only two initial conditions, $ig_n^F(0, 0) = \sum_\alpha K^\alpha \langle \hat{\sigma}_n^\alpha(0) \rangle + S + \frac{1}{2}$ and $g_n^\rho = iK^0$. These initial conditions also ensure that the EV of Schwinger boson constraint in Eq. (5) is satisfied at time $t = 0$, and, therefore, at all later times due to the symmetries of the SKFT action in real time. In our numerical integration scheme, the deviations of the EV of the Schwinger boson constraint are less than 10^{-14} [Fig. 10(f)]. However, the Schwinger boson constraint relates *operators*, which implies infinite constraints in terms of EVs, namely,

$$\langle \hat{a}_n^{(1)\dagger} \hat{a}_n^{(1)} + \hat{a}_n^{(2)\dagger} \hat{a}_n^{(2)} \rangle = 2S, \quad (28a)$$

$$\langle (\hat{a}_n^{(1)\dagger} \hat{a}_n^{(1)} + \hat{a}_n^{(2)\dagger} \hat{a}_n^{(2)})^2 \rangle = (2S)^2, \quad (28b)$$

$$\langle (\hat{a}_n^{(1)\dagger} \hat{a}_n^{(1)} + \hat{a}_n^{(2)\dagger} \hat{a}_n^{(2)})^3 \rangle = (2S)^3, \quad (28c)$$

and so on. But, a Gaussian initial density matrix forces the left-hand sides of Eqs. (28b) and (28c) to vanish at time $t = 0$. This erroneous initial value is con-

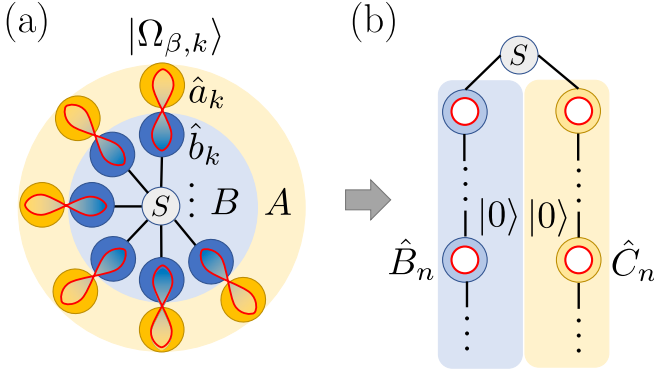


FIG. 3. (a) Illustration of how thermofield purification of the initial thermal state of the bath entangles each bath eigenmode with an ancilla. The geometry of interactions of the spin S with the bath modes is a star. (b) After performing a Bogoliubov transformation and orthogonal polynomial tridiagonalization we arrive at a two chain geometry ideal for MPS calculations.

served throughout the time evolution, allowing artificial virtual processes outside of the physical Hilbert space to potentially contribute to the discrepancy between SKFT+2PI and numerically exact benchmark results.

D. Tensor network approach to non-Markovian dynamics

For the spin-boson model [Eq. (1)] at low temperatures, we use TEDOPA, based on an MPS description of a thermofield-chain-mapped system [59, 67] to benchmark [Figs. 4(a),(c) and 5(a),(c)] our results from SKFT+2PI. An MPS is a representation of an arbitrary pure state as a product of local tensors given by [122]

$$|\psi\rangle = \sum_{s_1, \dots, s_N} A_1^{s_1} \dots A_{N-1}^{s_{N-1}} A_N^{s_N} |s_1 \dots s_N\rangle, \quad (29)$$

where $A_j^{s_i}$ is a $\chi_j \times \chi_{j+1}$ matrix (with $\chi_1 = \chi_N = 1$ fixed) for the j th local degree of freedom possessing a d_j dimensional Hilbert space. The bond dimension χ_j is a crucial parameter controlling the expressiveness of the MPS ansatz and is directly related to the maximum bipartite entanglement it can support.

In order to represent the equilibrium state of the bath in the form of a pure state MPS, we use thermofield purification in which the finite temperature of the bath is encoded in two different baths at zero temperature [123]. The thermal state of a bosonic bath at inverse temperature $\beta = 1/k_B T$ is given by

$$\hat{\rho}_\beta = \otimes_k \left(\sum_{n=0}^{\infty} \sqrt{\frac{e^{-\beta n \omega_k}}{Z_k}} |n\rangle \langle n|_k \right), \quad (30)$$

where $Z_k = (1 - e^{-\beta \omega_k})^{-1}$. By introducing an identical auxiliary system A with canonical operators $\hat{a}_k^\dagger, \hat{a}_k$ we

can define the thermofield double state as a purification of $\hat{\rho}_\beta$, given by

$$\begin{aligned} |\Omega_\beta\rangle &= \otimes_k |\Omega_{\beta,k}\rangle = \otimes_k \left(\sum_{n=0}^{\infty} \sqrt{\frac{e^{-\beta n \omega_k}}{Z_k}} |n_B\rangle_k \otimes |n_A\rangle_k \right) \\ &= \exp \left(\sum_k \theta_k (\hat{b}_k \hat{a}_k - \hat{b}_k^\dagger \hat{a}_k^\dagger) \right) |\text{vac}\rangle, \end{aligned} \quad (31)$$

where $|\text{vac}\rangle$ is bosonic vacuum state; $\theta_k = \text{atanh}(e^{-\beta \omega_k/2})$; and $\hat{\rho}_\beta = \text{Tr}_A(|\Omega_\beta\rangle \langle \Omega_\beta|)$ is obtained by partial trace over the states of auxiliary system A . The state $|\Omega_\beta\rangle$ is the vacuum for the modes

$$\hat{c}_{1,k} = e^{-iG} \hat{b}_k e^{iG} = \cosh(\theta_k) \hat{b}_k - \sinh(\theta_k) \hat{a}_k^\dagger, \quad (32)$$

$$\hat{c}_{2,k} = e^{-iG} \hat{b}_k e^{iG} = \cosh(\theta_k) \hat{a}_k - \sinh(\theta_k) \hat{b}_k^\dagger, \quad (33)$$

where $G = i \sum_k \theta_k (\hat{b}_k^\dagger \hat{a}_k^\dagger - \hat{a}_k \hat{b}_k)$ is a thermal Bogoliubov transformation. We then use as the ancilla system Hamiltonian $H_A = - \sum_k \omega_k \hat{a}_k^\dagger \hat{a}_k$ such that in the new basis the extended Hamiltonian is given by

$$\begin{aligned} \hat{H} &= \frac{\omega_q}{2} \hat{\sigma}^z + \frac{\Delta}{2} \hat{\sigma}^x + \sum_k \omega_k (\hat{c}_{1,k}^\dagger \hat{c}_{1,k} - \hat{c}_{2,k}^\dagger \hat{c}_{2,k}) \\ &+ \hat{\sigma}^z \sum_k \left(\frac{g_{1k}}{2} (\hat{c}_{1,k} + \hat{c}_{1,k}^\dagger) + \frac{g_{2k}}{2} (\hat{c}_{2,k} + \hat{c}_{2,k}^\dagger) \right), \end{aligned} \quad (34)$$

where $g_{1k} = g_k \cosh(\theta_k)$ and $g_{2k} = g_k \sinh(\theta_k)$.

As it stands, this setup has a star geometry in which the spin interacts with each eigenmode of the bath, as illustrated graphically in Fig. 3(a). Within the 1D of an MPS, this corresponds to long-ranged interactions, which are more difficult to handle in this formalism. For this reason, we map via continuous mode tridiagonalization the two zero temperature star geometry baths into two 1D tight binding chains, each coupled to the system spin [67], as shown in Fig. 3(b). In the continuum representation, these two baths are characterized by spectral densities $\mathcal{J}_1(k) = [1 + n_{\text{BE}}(k)] \mathcal{J}(k)$ and $\mathcal{J}_2(k) = n_{\text{BE}}(k) \mathcal{J}(k)$ where $n_{\text{BE}}(k)$ is the Bose-Einstein distribution function, which we use to define new bosonic operators \hat{B}_n and \hat{C}_n such that

$$\hat{c}_{1,k} = \sum_n U_{1,n}(k) \hat{B}_n, \quad \hat{c}_{2,k} = \sum_n U_{2,n}(k) \hat{C}_n. \quad (35)$$

Here, $U_{j,n}(k) = g_j(k) \pi_{j,n}(k) / \rho_{j,n}$ for $j = 1, 2$ and $\pi_{j,n}(k)$ are monic orthogonal polynomials that obey

$$\int_0^\infty dk \mathcal{J}_j(k) \pi_{j,n}(k) \pi_{j,m}(k) = \rho_{j,n}^2 \delta_{n,m}, \quad (36)$$

with $\rho_{j,n}^2 = \int_0^\infty dk \mathcal{J}_j(k) \pi_{j,n}^2(k)$ [59]. This description simplifies significantly at zero temperature, as $\mathcal{J}_1(k) = 0$, so only one chain is needed. Using a finite cutoff of M

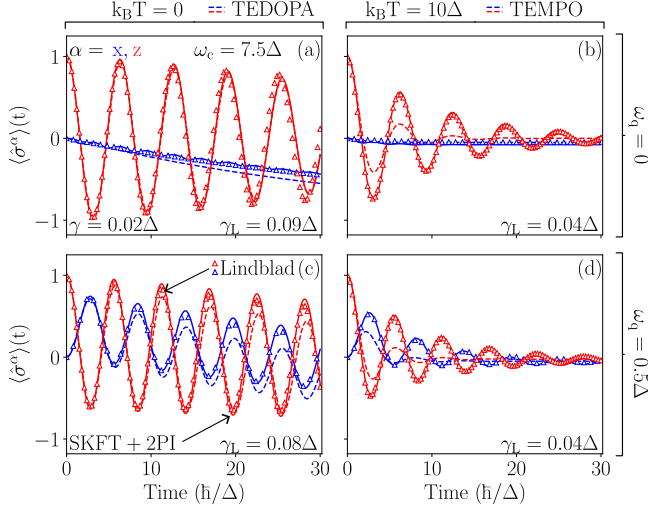


FIG. 4. Time dependence of spin expectation values $\langle \hat{\sigma}^\alpha \rangle$ of the spin-boson model [Eq. (1)] computed from our SKFT+2PI (solid lines) approach vs. standard Lindblad QME (triangles) or TN methods (dashed lines) with bath cutoff frequency $\omega_c = 7.5\Delta$ in the *weak* system-bath coupling regime, $\gamma \ll \Delta$, where the system dynamics is expected [7] to be *Markovian* [80, 81] for the chosen Ohmic bath [$s = 1$ in Eq. (2)]. Panels in different columns and rows use different values of temperature T and two-level splitting ω_q , respectively. For $k_B T = 0$, the chosen TN method is TEDOPA, while for $k_B T = 10\Delta$, we use TEMPO (see Secs. II D and III for details). The SKFT+2PI and TN-computed benchmark results follow each other closely for the chosen $\gamma = 0.02\Delta$, while the system-bath coupling in Eqs. (38) and (39) for the Lindblad QME, γ_L , must be adjusted by increasing it to match the other two calculations (this points to artifacts of the Lindblad QME derived [2] for the spin-boson model).

modes for the mapping, we have

$$\begin{aligned} \hat{H} = & \frac{\omega_q}{2} \hat{\sigma}^z + \frac{\Delta}{2} \hat{\sigma}^x + \hat{\sigma}^z \left(\rho_{1,0}(B_0 + B_0^\dagger) + \rho_{2,0}(C_0 + C_0^\dagger) \right) \\ & + \sum_{n=0}^M \left(\alpha_{1,n} \hat{B}_n^\dagger \hat{B}_n - \alpha_{2,n} \hat{C}_n^\dagger \hat{C}_n + \sqrt{\beta_{1,n+1}} \hat{B}_{n+1}^\dagger \hat{B}_n \right. \\ & \left. - \sqrt{\beta_{2,n+1}} \hat{C}_{n+1}^\dagger \hat{C}_n + \text{H.c.} \right), \end{aligned} \quad (37)$$

where the coefficients $\alpha_{j,n}$ and $\beta_{j,n}$ are defined through the recurrence relation $\pi_{j,n+1}(k) = (k - \alpha_{j,n})\pi_{j,n}(k) - \beta_{j,n}\pi_{j,n-1}(k)$, with $\pi_{j,-1}(k) = 0$. These chain parameters were generated using the ORTHPOL package [124]. Generically, they are found to quickly converge to constants $\alpha_{i,n} \rightarrow \alpha_i$, $\beta_{i,n} \rightarrow \beta_i$. Using the Lieb-Robinson bounds [95, 96], sites further than $\sim \tau\beta_i$ have a negligible effect on the system dynamics up to time τ , giving a well-defined measure of the length of bath chains we need. In this sense, the discretization generated by orthogonal polynomials is exact up to a finite time. To time evolve the MPS, we use the two-site variant of the TDVP [125–128] which dynamically updates the MPS bond dimensions to maintain a desired level of precision.

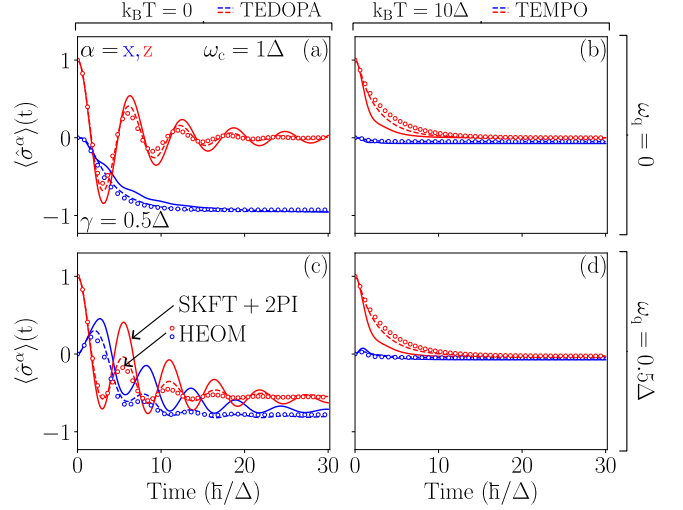


FIG. 5. The same information as in Fig. 4, but for bath cutoff frequency $\omega_c = 1\Delta$ and in the *strong* system-bath coupling regime, $\gamma = 0.5\Delta$, where the system dynamics is expected to be *non-Markovian* [80, 81] for the chosen [7] Ohmic bath [$s = 1$ in Eq. (2)]. Different columns and rows of panels use different values of temperature T and two-level splitting ω_q [Eq. (1)], respectively. Note that standard HEOM calculations [79] cannot be conducted at $k_B T = 0$ temperature, so in the left column of panels we use higher temperature $k_B T = 0.1\Delta$ in HEOM calculations instead of $k_B T = 0$ [as marked on the top of panel (a)] employed in SKFT+2PI and TN-based calculations.

E. HEOM approach to non-Markovian dynamics

The HEOM algorithm [79], initially developed for problems in quantum chemistry [129], is a widely used method for solving QMEs of open quantum systems, such as the spin-boson model [Eq. (1)], with arbitrary system-bath coupling. However, in its original formulation [79, 129] it requires finite temperature, $T > 0$ [76, 77, 82, 83]. The non-perturbative treatment of interaction with the bath is achieved by introducing a hierarchy of auxiliary density matrices which encode system-bath correlations and entanglement [79, 130]. This hierarchy relies on the expansion of the bath correlation function into an exponential form. The limitations of the HEOM method are well known [76, 77, 82, 83] and arise from the truncation of either the number of auxiliary matrices (a stronger system-bath coupling requires a higher hierarchy cutoff), or the truncation in the exponential decomposition of the bath correlation (typically, lower temperature requires a higher number of terms in the expansion). The exact exponential expansion of an arbitrary spectral density $\mathcal{J}(\omega)$ of the bath is not known. We fit the spectral density in Eq. (2) using a sum of up to four underdamped [79] spectral densities whose exponential expansion is well known [131]. In order to guarantee convergence, we ran simulations varying the hierarchy cutoff, up to a maximum of 11. In addition, we also ad-

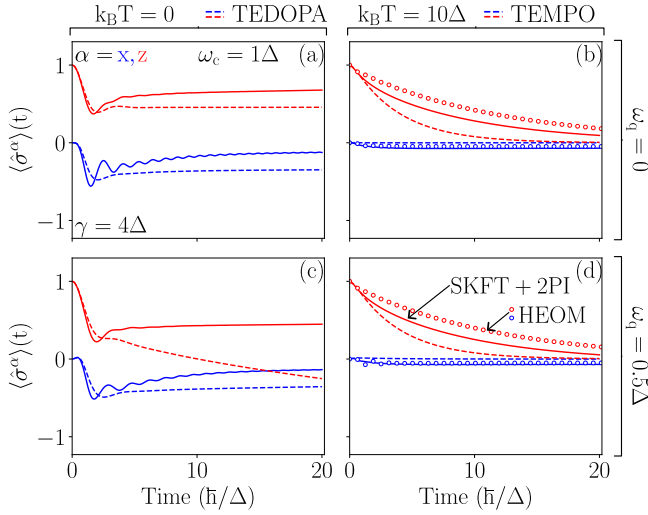


FIG. 6. The same information as in Fig. 5, but for bath cutoff frequency $\omega_c = 1\Delta$ and in the *ultrastrong* system-bath coupling regime, $\gamma = 4\Delta$, where the system dynamics is expected to be *highly non-Markovian* [80, 81] for the chosen [7] Ohmic bath [$s = 1$ in Eq. (2)]. The ultrastrong system-bath coupling induces localization of the spin for $k_B T = 0$, i.e., $\langle \hat{\sigma}^z \rangle$ plateaus at a finite noninteger value. This nonperturbative behavior of plateau reached in the long time limit is captured by SKFT+2PI, but the specific value of the plateau differs from TN-computed benchmark at low temperatures.

just the number of exponential terms, using a maximum of 16 terms for the lowest temperature case $k_B T = 0.1\Delta$ [Fig. 5]. All such calculations were performed using the HEOM extension [132] of the QuTiP [133, 134] package.

F. Lindblad QME approach to Markovian dynamics

In the weak system-bath coupling regime of the spin-boson model [Eq. (1)], where the system (i.e., spin) dynamics is expected to be Markovian [80, 81], it is assumed that Lindblad QME [6, 7]

$$\frac{d\hat{\rho}}{dt} = -i[\hat{H}_S, \hat{\rho}] + \sum_{i=0}^2 \hat{L}_i \hat{\rho} \hat{L}_i^\dagger - \frac{1}{2} \{ \hat{L}_i^\dagger \hat{L}_i, \hat{\rho} \}, \quad (38)$$

can accurately capture the open quantum system dynamics. Here \hat{H}_S is the Hamiltonian of an isolated spin, composed of the first two terms on the RHS of Eq. (1); $\hat{\rho}$ is the spin density matrix [17]; and \hat{L}_i is a set of three Lindblad operators [6, 7] which account for the presence of the bosonic bath. Those three \hat{L}_i operators for the spin-boson model can be expressed [2] in the energy eigenbasis

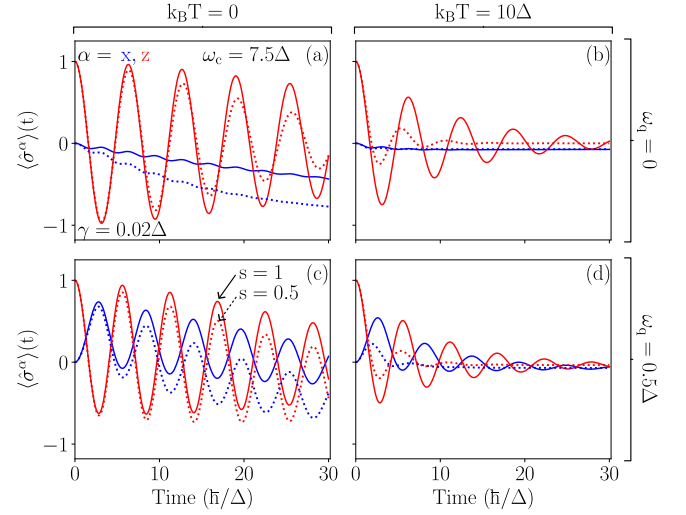


FIG. 7. Time dependence of spin expectation values $\langle \hat{\sigma}^\alpha \rangle$ computed from SKFT+2PI for bosonic bath with Ohmic (solid lines) or sub-Ohmic (dotted lines) spectral density, i.e., $s = 1$ or $s = 0.5$ in Eq. (2), respectively. Other parameters are the same as in the weak system-bath coupling regime of Fig. 4. Note that solid lines are identical to solid lines in Fig. 4, which are plotted here for easy comparison.

of \hat{H}_S , $\hat{H}_S |\pm\rangle = E_\pm |\pm\rangle$, of \hat{H}_S as

$$\hat{L}_0 = \sqrt{J(\Delta E)[1 + n_{\text{BE}}(\Delta E)][\langle +|\hat{\sigma}_z|-\rangle]^2/4}|-\rangle\langle +|, \quad (39a)$$

$$\hat{L}_1 = \sqrt{J(\Delta E)n_{\text{BE}}(\Delta E)[\langle +|\hat{\sigma}_z|-\rangle]^2/4}|+\rangle\langle -|, \quad (39b)$$

$$\hat{L}_2 = \sqrt{\gamma_L T \langle -|\hat{\sigma}_z|-\rangle \langle +|\hat{\sigma}_z|+\rangle/2}|-\rangle\langle -|, \quad (39c)$$

where $\Delta E = E_+ - E_-$ is the energy difference of the two levels, and γ_L is the system-bath coupling we have to adjust [Fig. 4] when using Lindblad QME.

III. RESULTS AND DISCUSSION

A. Spin-boson model

Let us re-emphasize that the spin-boson model in Eq. (1) is the particular case of the more general Hamiltonian in Eq. (3) in which the number of spins $N_S = 1$, $\mathbf{b} = (\Delta, 0, \omega_q)$, $J_{11}^{\alpha\beta} = 0$, and $g_{n=1,k}^z$ are the only nonzero spin-bath couplings. For clarity of notation, we suppress the subscript $n = 1$ when discussing results concerning a single-spin system. The dynamics of spin EVs is obtained from

$$\langle \hat{\sigma}^\alpha \rangle(t) = \frac{1}{2} \text{Tr}_S[g^F(t, t)K^\alpha], \quad (40)$$

and plotted in Figs. 4, 5, and 6 for the Ohmic bath [$s = 1$ in Eq. (2)], as well as in Fig. 7 for sub-Ohmic bath [$s = 0.5$ in Eq. (2)].

In Fig. 4 we focus on the Markovian regime. Note that delineating a precise boundary between Markovian and non-Markovian regimes requires considering [80, 81] the interplay of several parameters in the spin-boson model. Nevertheless, the most important ones are the magnitude of the system-bath coupling γ and the cutoff frequency ω_c [7]. Therefore, in Fig. 4 we employ small $\gamma = 0.02\Delta$ and high $\omega_c = 7.5\Delta$ to ensure the Markovian dynamics [80]. The Markovian nature of such regime is reflected in the irreversible decay of purity [orange solid line in Fig. 8] of the mixed quantum state of spin $S = 1/2$. Since the spin density matrix $\hat{\rho}$ and the Bloch vector $\mathbf{P} = (P^x, P^y, P^z)$ are in one-to-one correspondence [17]

$$\hat{\rho} = \frac{1}{2} \left(\hat{I} + \sum_{\alpha} P^{\alpha} \hat{\sigma}^{\alpha} \right), \quad (41)$$

where \hat{I} is the unit operator in the spin space, we use $|\mathbf{P}|$ as a proxy of the purity. The standard purity $\text{Tr} \hat{\rho}^2$ is a function of $|\mathbf{P}|$, where $|\mathbf{P}| = 1$ signifies fully coherent or pure quantum state of spin $S = 1/2$ or qubit, while $0 \leq |\mathbf{P}| < 1$ denotes mixed quantum states. In the Markovian regime, we find excellent agreement between SKFT+2PI (solid lines) and Lindblad-QME-computed results (triangles) in Fig. 4. However, such a match is *ensured only* by adjusting the system-bath coupling in the Lindblad QME, thereby pointing to an artifact of standard Lindblad QME [2] since our SKFT+2PI results independently and closely match the results of TN calculations (dashed lines in Figs. 4 and 5) employing the same coupling γ . Our TN calculations for the $k_B T = 0$ case used TEDOPA [59, 64, 67], whereas for the higher temperature $k_B T = 10\Delta$ we switch to TEMPO [40, 63].

Outside the Markovian regime, the Lindblad QME cannot capture the memory effects of the bath, which can cause the revival of quantum properties. Such revival is exemplified by the purity $|\mathbf{P}|$ of the mixed quantum state of spin initially decaying in Figs. 8(a) and 8(c), as the signature of decoherence [18], but later increasing towards $|\mathbf{P}| = 1$ of the pure state at $t = 0$ as the signature of re-coherence [4]. In the non-Markovian regime of Fig. 5, we replace the Lindblad QME benchmark with HEOM and TN calculations benchmarks. The non-Markovian regime [Fig. 5] is induced by using a strong system-bath coupling $\gamma = 0.5\Delta$ and low cutoff frequency $\omega_c = \Delta$, while keeping the Ohmic bath as in Fig. 4. We find that for zero temperature [Figs. 5(a),(c)], the TEDOPA results [dashed lines in Fig. 5] follow closely those from HEOM [circles in Fig. 5], on the proviso that we use slightly higher temperature $k_B T = 0.1\Delta$ in the HEOM calculations. The necessity for such *ad hoc* fix of standard HEOM calculations stems from the fact that they *cannot* [76, 77, 82] handle $k_B T = 0$ limit. The spin EVs computed from our SKFT+2PI are capable in tracking these benchmark results, but they appear as if their damping is slightly smaller [compare solid lines from SKFT+2PI to circles from HEOM and dashed lines from TEDOPA calculations Fig. 5(c)]. This goes against naïve expectation of

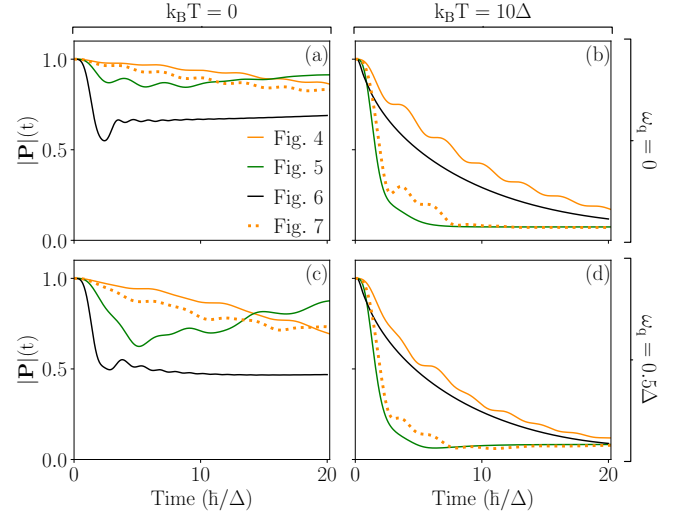


FIG. 8. Time dependence of purity $|\mathbf{P}| = \sqrt{\sum_{\alpha} \langle \hat{\sigma}_{\alpha} \rangle^2}$ of mixed quantum state of spin $S = 1/2$ from SKFT+2PI-computed curves in Figs. 4, 5, 6 and 7. Orange, green, and black solid lines are for the case of an Ohmic bath [Fig. 4, Fig. 5 and Fig. 6], while orange dotted line is for the case of a sub-Ohmic bath [Fig. 7].

higher damping effectively emerging [114, 120, 135] in closed quantum systems due to neglected Feynman diagrams in 2PI resummation and neglected initial non-Gaussian correlations.

We additionally examine the non-Markovian regime for the case of an ultrastrong system-bath coupling $\gamma = 4\Delta$ [Fig. 6], while keeping the remaining parameters the same as in Fig. 5. At zero temperature in this regime, the spin-boson transitions to a localized phase [136, 137] occurs, which is characterized by long-range correlations in time and the EV $\langle \hat{\sigma}^z \rangle$ saturating at a finite value despite the presence of the dissipative environment and regardless of two-level splitting ω_q . Such saturation is observed in both the TEDOPA and our SKFT+2PI results, demonstrating the ability of SKFT+2PI to capture highly non-perturbative effects. However, for vanishing two-level splitting, $\omega_q = 0$ [Fig. 6(a)], SKFT+2PI only matches TEDOPA qualitatively, while differing in their long-time limit. The discrepancy is more severe for $\omega_q = 0.5\Delta$ [Fig. 6(c)]. Such discrepancy is likely caused by neglecting important non-Gaussian initial correlations, or spontaneous symmetry breaking of the fields. On the other hand, SKFT+2PI performs much better for high temperatures and ultrastrong coupling [Fig. 6(b) and 6(d)] than TN calculations like TEMPO, where the latter struggles to converge in the same regime. In fact, in this regime SKFT+2PI results are superior to TEMPO in matching the HEOM benchmark. Let us again emphasize that the standard version of HEOM cannot [76, 77, 82] handle zero temperature $k_B T = 0$ which is critical for the transition to the localized phase, and so its results are omitted from Figs. 6(a) and 6(c).

Finally, Fig. 7 demonstrates the ability of our

SKFT+2PI formalism to treat a variety of other system and bath parameters, such as the case of zero temperature and sub-Ohmic bath that is considered particularly challenging [61, 68–71, 76]. For this purpose, we compute via SKFT+2PI the spin EVs for a sub-Ohmic bath, with $s = 0.5$ in Eq. (2), while using the same parameters as in the weak system-bath coupling regime of Fig. 4 for the sake of comparing Ohmic vs. sub-Ohmic cases. The results in Fig. 7 show faster decrease of the spin EVs when the bath is sub-Ohmic. However, the purity in sub-Ohmic case [orange dotted line in Fig. 8] *does not* decay monotonically as in the case of Markovian regime for Ohmic bath [orange solid line in Fig. 8]. Instead, it saturates at a finite value at zero temperature, akin to the Ohmic non-Markovian case [green and black lines in Fig. 8 obtained using SKFT+2PI from Fig. 5 and Fig. 6]. Moreover, at high temperature, the purity of spin state in the sub-Ohmic regime closely resembles the time evolution of it in the strong system-bath coupling (i.e., non-Markovian) regime, except for small revivals [orange dotted curve in Figs. 8(b),(d)] at intermediate time scales. Thus, Fig. 8 illustrates the difficulties [61, 68–71, 76] posed by the sub-Ohmic case because of the skew towards low bath frequencies [Fig. 1(a)] which enhance the memory effects of the bath. This makes it possible for the non-Markovian features to show up *despite* weak system-bath coupling. In other words, the standard lore [7] that system-bath coupling is the primary controller of the boundary between Markovian and non-Markovian regimes, with low temperature making the non-Markovian effects more pronounced [60, 61, 73], requires careful reexamination in the case of the spin-boson model. This archetypical model of open quantum systems can exhibit complex diagram of dynamical regimes [80, 81] due to interplay of several parameters in Eqs. (1) and (2). Thus, we find that weak system-bath coupling and a sub-Ohmic bath [Fig. 7] can be as challenging as strong system-bath coupling and an Ohmic bath [Fig. 5]. Nevertheless, our SKFT+2PI demonstrates ability to handle many different combinations of parameters, as well as long evolution times, within a *single unified framework*.

B. Two-spin correlators in spin-boson model

The order parameter related to the quantum phase transition [136, 137] of the spin-boson model [Eq. (1)] is a two-spin correlator that is zero in the delocalized phase [Figs. 4, 5 and 7] but abruptly acquires a finite value in the localized phase [Fig. 6]. We demonstrate that such manifestly nonperturbative behavior is still amenable to our SKFT+2PI treatment employing 2PI resummation of Feynman diagrams $1/N$ expansion. Specifically, the order parameter is the time integral,

$$m^2 = \int dt iC^{zz,F}(t, 0), \quad (42)$$

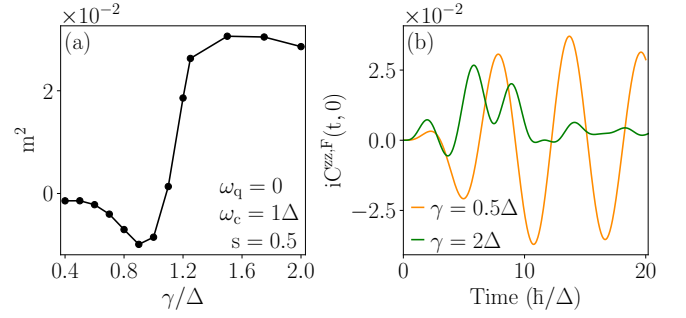


FIG. 9. (a) Order parameter [Eq. (42)] of the quantum phase transition [136, 137] of the spin-boson model as a function of the system-bath coupling γ . The transition is signified by a kink at the critical coupling $\gamma_c \approx \Delta$. (b) Correlation between spin at time t and the initial state for couplings in the delocalized and localized phase (orange and green lines, respectively).

of the statistical component [as obtained from Eq. (23)] of the dynamical (because of usage of two times) connected two-spin correlator [137]

$$C_{nn'}^{\alpha\beta}(t, t') = i \langle \sigma_n^\alpha(t) \sigma_{n'}^\beta(t') \rangle - i \bar{\sigma}_n^\alpha(t) \bar{\sigma}_{n'}^\beta(t'). \quad (43)$$

We extract this quantity from SKFT+2PI approach by using the mean-field propagator $\tilde{M}_{nn'}^{\alpha\beta}$ and by introducing a replica spin. Intuitively, the mean-field Λ_n^α is proportional to a sum of neighboring spin EVs [Eqs. (18b) and (40)], so the mean-field propagator,

$$M_n^\alpha(t, t') \propto \langle \Lambda_n^\alpha(t) \Lambda_{n'}^\beta(t') \rangle \quad (44)$$

should be related to the two-spin correlator. Rigorously, the mean-field propagator can be generated as a functional derivative

$$\left. \frac{\delta^2 Z[\Phi, \eta]}{\delta \eta_n^\alpha(t) \delta \eta_{n'}^\beta(t')} \right|_{\eta=0} = -i M_{nn'}^{\alpha\beta}(t, t') - \bar{\Lambda}_n^\alpha(t) \bar{\Lambda}_{n'}^\beta(t'), \quad (45)$$

where the generating functional is given by

$$Z[\Phi, \eta] = \int \mathcal{D}\Phi e^{iS[\Phi] + i \int_c \sum \eta_n^\alpha \Lambda_n^\alpha}. \quad (46)$$

Here η_n^α is an external source and the action $S[\Phi]$ is in the form of Eq. (14). By first integrating out the mean-field, which now couples to the external source, and then performing the functional derivative in Eq. (45), we find that the mean-field propagator is indeed proportional to the connected two-spin correlator,

$$C_{nn'}^{\alpha\beta}(t, t') = -\tilde{M}_{nn'}^{\alpha\beta}(t, t'). \quad (47)$$

A similar procedure, but based on the bath propagator D_n^α , could also be executed. However, the additional requirement on this derivation route is to carefully invert convolutions on the Schwinger-Keldysh closed time contour involving the bath kernel Ξ_n^α . This is quite cumbersome and prevents finding a simple solution akin to

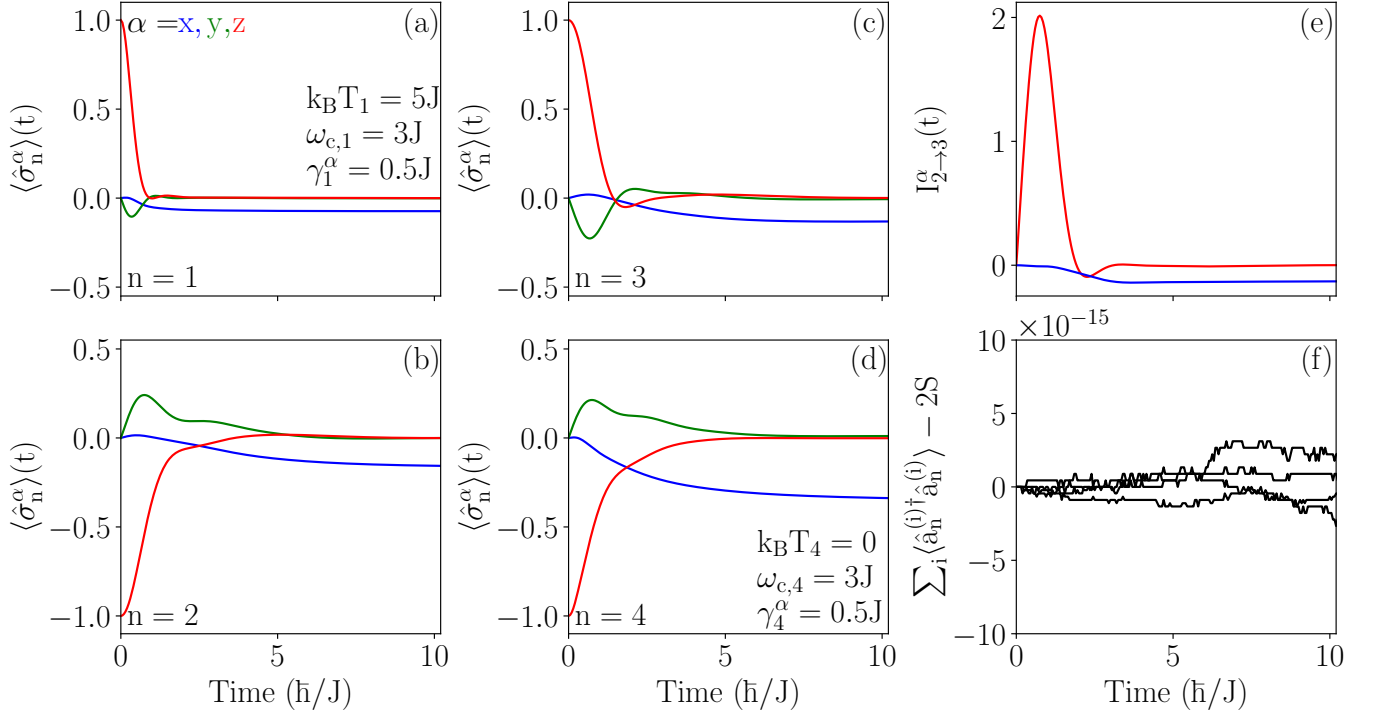


FIG. 10. (a)–(d) Time dependence of the spin expectation values $\langle \hat{\sigma}_n^\alpha \rangle$ obtained from SKFT+2PI for each site n of the spin-chain-boson model [Eq. (3) and Fig. 1(b)]. (e) Time dependence of components of the bond spin current [Eq. (48)] between sites $n = 2$ and $n' = 3$. (f) Time dependence of the Schwinger boson constraint $\langle \hat{a}_n^{(1)\dagger} \hat{a}_n^{(1)} + \hat{a}_n^{(2)\dagger} \hat{a}_n^{(2)} \rangle = 2S$ for spins at all $n = 1, 2, 3, 4$ sites, demonstrating that it is conserved during time evolution.

Eq. (47). Thus, we compute two-spin correlators exclusively via simpler Eq. (47), which requires nonzero exchange coupling $J_{nn'}^{\alpha\beta} \neq 0$ between the spins σ_n^α and $\sigma_{n'}^\beta$. However, this prevents direct access to the same-site two-spin correlator $C_{nn}^{\alpha\beta}(t, t')$, as required for calculating the order parameter of the spin-boson model. Hence, we solve this problem by introducing a replica spin with identical initial state. For this procedure to work, such replica spin must be weakly and ferromagnetically coupled to $\hat{\sigma}_{n=1}$ to prevent modifying its trajectory. Then, the two-spin correlator between the spin and its replica mimics the original same-site two-spin correlator $C_{11}^{\alpha\beta}(t, t')$.

Figure 9(a) shows the order parameter as a function of the system-bath coupling γ between an unbiased ($\omega_q = 0$) system and a sub-Ohmic $s = 0.5$ bath with small cutoff frequency $\omega_c = \Delta$. On the delocalized side of the transition, the order parameter vanishes due to the oscillations of the two-spin correlator as a function of time [orange line in Fig. 9(b)]. In contrast, on the localized side of the quantum phase transition in the spin-boson model, the two-spin correlator is almost always positive [green line in Fig. 9(b)], signifying that spin EV is saturated at a nonzero value, hence the meaning of “localized” terminology. For the chosen bath parameters, we find the critical coupling to be $\gamma_c \approx \Delta$, as the non-thermally-related parameter whose tuning drives the quantum phase tran-

sition [138].

C. Spin-chain-boson model

Taking into account that a chain of mutually-interacting open quantum systems, each of which also interacts with a common or individual environments, is a challenging problem [39–43] for very recent efforts to develop approaches for non-Markovian dynamics of systems with larger Hilbert space than two-dimensional one of a single spin $S = 1/2$ within the spin-boson model, in this Section we consider spin-chain-boson model described by Eq. (3) and illustrated in Fig. 1(b). Interestingly, prior studies of open quantum magnets in equilibrium have found that ordinarily-forbidden long range order in 1D quantum spin chains can be stabilized by the presence of Ohmic and sub-Ohmic baths [139]. Thus, having a formalism that can examine non-Markovian dynamics of standard or exotic quantum magnets (such as quantum spin liquids [140]), or systems of interacting qubits [35, 36] including their arrangements in three dimensional geometries [44], is of great contemporary interest as they are necessarily interacting with a dissipative environment at finite temperature in experiments [141].

Our spin chain [Fig. 1(b)] contains four quantum spins $S = 1/2$ with antiferromagnetic (AF) exchange coupling

between the nearest neighbors in which the spins at the ends couple to independent sets of three bosonic baths (one for each spin component $\alpha = x, y, z$). Such system is described by the general Hamiltonian in Eq. (3) by setting the exchange couplings $J_{n,n+1}^{\alpha\beta} = J_{n,n-1}^{\alpha\beta} = J\delta^{\alpha\beta}$, and the spin-bath couplings $g_{1k}^\alpha = g_{4k}^\alpha = 0.1J$. The temperature of the baths coupled to the spin $n = 1$ and $n = 4$ are set to $k_B T = 5J$ and $k_B T = 0$, respectively, with all other parameters being the same for simplicity. An external magnetic field along the x -axis is included by using $\mathbf{h} = (J, 0, 0)$ in Eq. (3).

The dynamics of the EVs of the four spins are shown in Fig. 10(a)–10(d), respectively. Note that in this case we do not have any benchmarks from either HEOM, because of too many spins; or from TN calculations (i.e., TEDOPA or TEMPO algorithms employed in the case of spin-boson model in Figs. 4, 5, 6), because of difficulty we find when using the respective packages [40] in handling multiple baths coupled to the three components of vector operator of spin localized at a given site of the chain. Due to necessity to employ Gaussian initial state [27] in current implementation of SKFT, we start from the Néel ket $|\uparrow\downarrow\uparrow\downarrow\rangle$ as the initial and *unentangled* state in which $\langle\hat{\sigma}_1^z\rangle = \langle\hat{\sigma}_3^z\rangle = 1$ and $\langle\hat{\sigma}_2^z\rangle = \langle\hat{\sigma}_4^z\rangle = -1$. The fact that dynamics of four EVs tends to zero or small value $|\langle\hat{\sigma}_n\rangle| \ll 1$ signifies nonzero entanglement of a mixed quantum many-body state [93] which is made possible by the non-Markovian nature of open quantum spin chain dynamics.

The open AF quantum spin chain with different temperatures of the baths connected at its boundaries [142] will exhibit both nonequilibrium spin and heat currents [143, 144]. Since the total heat current requires three-spin correlators [143, 144], which are inaccessible from our current implementation of our SKFT+2PI formalism, we compute only spin current as an illustration. The α -component of the bond spin current between two spins n, n' is expressed as [143]

$$I_{n \rightarrow n'}^\alpha(t) = 2iJ \sum_{\beta\gamma} \epsilon_{\alpha\beta\gamma} C_{nn'}^{\beta\gamma,F}(t, t), \quad (48)$$

in terms of two-spin correlators [Eq. (43) at equal times], where $\epsilon_{\alpha\beta\gamma}$ is the Levi-Civita symbol. The bond spin currents $I_{n \rightarrow n'}^\alpha$, out of which we plot only $I_{2 \rightarrow 3}^x$ in Fig. 10, have a finite value in the steady state because of externally applied magnetic field \mathbf{h} along the x -axis. Furthermore, despite the absence of its component along the z -axis, there is a transient z -component of the bond spin currents, $I_{n \rightarrow n'}^z$, generated by the presence of bosonic baths at the chain boundaries. These transient oscillations can be even long lived due to finite-size effects. However, Feynman diagrams beyond those included in 2PI effective action and/or initial non-Gaussian correlations introduce artifactual damping that accelerates their decay in Fig. 10(e).

IV. CONCLUSIONS AND OUTLOOK

A. Conclusions

In conclusion, we construct a promising field-theoretic approach to driven-dissipative many-body systems, as one of the most challenging unsolved problems in many-body quantum physics [145], which can tackle variety of dynamical regimes and system geometries or dimensionalities [44, 45]. In contrast, numerically exact benchmarks employed on the spin-boson model as a standard testbed [73] require changing the method (such as HEOM [79] vs. different flavors of TN approaches [40, 41]) depending on the chosen parameters of the model. Furthermore, we also demonstrate how our SKFT+2PI framework can handle *multiple* interacting quantum spins and baths in the *non-Markovian* regime where very recently developed TN methods for this frontier problem can encounter impediments due to transient entanglement barrier [90–92], even in the presence of dissipative environment [93], as well as due to complexity of the setup we choose in Fig. 1(b). In addition, usage of Schwinger bosons in our SKFT+2PI framework can handle arbitrary spin value S of interest to quantum spintronics [19–23] and quantum magnonics [45] or qudits in quantum computing [146]. The ability of our SKFT+2PI framework to closely track numerical exact results from TN calculations on the spin-boson model demonstrate that this approach is *nonperturbative* in the system-bath coupling. This achievement can be traced back to the usage of 2PI resummation of a class of infinitely many Feynman diagrams generated by the $1/N$ expansion (where N being the number of Schwinger bosons to which quantum spins are mapped) instead of conventional expansion in the system-bath coupling. Although $1/N$ expansions have been formulated in high energy physics long ago [54], it is only very recently understood [55] that their ability to capture nonperturbative physics stems from deep connection to resurgent transseries [52, 56] in the coupling constant. In addition, our SKFT+2PI offers a single framework which can handle arbitrary temperature, cutoff frequency of the bath, spectral content of the bosonic baths (i.e., Ohmic vs. sub-Ohmic vs. super-Ohmic) and exchange interaction in the case of many spins. Unlike widely used QMEs in open quantum system dynamics, where only the reduced density matrix is accessible as a function of time, both our SKFT+2PI framework and TN methods [40, 41] make possible computation of multitime two-spin correlators. For example, using such correlators, we are able to obtain order parameter [Fig. 9] of delocalized-localized quantum phase transition in the spin-boson model or nonequilibrium spin current [Fig. 10] in the spin-chain-boson model. We note that prior comparisons [103, 147] of perturbative expansions of Keldysh GFs in the coupling constant vs. TN-computed benchmarks find discrepancies quickly growing as the coupling constant is increased, no matter how many of such diagrams are self-consistently summed.

The numerical cost of solving integro-differential equations [Eq. (26) and Fig. 2] produced by SKFT+2PI formalism is quartic scaling in the number of time steps, but it could be lowered to linear (a topic of great contemporary interest in open quantum system dynamics [148]) by optimizing numerics. Moreover, the largest matrix (see Table I) required in solving the SKFT+2PI equations of motion in Eqs. (18) and (26) is of the size $3N_S \times 3N_S$ for N_S spins of arbitrary value S (instead of $(2S+1)^{N_S} \times (2S+1)^{N_S}$ matrices in brute force methods). Ability to solve problems of N_S spins of arbitrary value S , and in *arbitrary* geometry [1] or spatial dimensionality [44, 45] that are coupled to dissipative environment is of high demand for quantum spintronics [19–23] and quantum magnonics [45], where the spin value $S \geq 1/2$, as well as for quantum computing [44] where $S = 1/2$ for qubits [35, 36] and $S > 1/2$ for qudits [146].

B. Outlook

We note that combination of SKFT, 2PI and $1/N$ expansion (where N is the number of Schwinger bosons) for many-body quantum spin systems which are *closed* has been formulated [47, 48] in order to be able to study far-from-equilibrium dynamics in three spatial dimensions, where TN methods able to encode efficiently low-entangled quantum many-body states become inapplicable [1, 149, 150], as well as for arbitrary exchange coupling. However, these studies did not benchmark their theory on low-dimensional spin systems where TN methods are applicable [1, 149, 150] and provide numerically (quasi)exact reference point. With such benchmarking performed on, e.g., closed quantum spin chains, one would discover that SKFT+2PI for closed quantum spin systems [47, 48] fails after relatively short evolution

time. In contrast, our formulation of SKFT+2PI for *open* quantum spin systems produces nonperturbative results in system-bath or spin-spin exchange couplings that can track accurately benchmarks from TN methods. The failure of SKFT+2PI for closed quantum spin systems requires further scrutiny, and we believe it originates from initial conditions restricted to Gaussian density matrix, as well as possibly from neglected Feynman diagrams [114, 120, 135] acting as effective damping. Thus, the fact that our SKFT+2PI for *open* quantum spin systems works so well suggests that presence of dissipative environment alleviates these issues. Nevertheless, in some pockets of space of dynamical regimes, such as at ultrastrong system-bath coupling [Fig. 6(c)] we do find discrepancy between our SKFT+2PI and TN benchmarks for the spin-boson model. Since all approximations we made in this case are controllable, our results could be further improved, such as by: coupling of 2PI with additional resummation techniques [49, 52, 55]; going to higher loop order within n PI effective action [151, 152] where $n > 2$; and solving the fundamental problem [153] of how to include non-Gaussian initial states into SKFT. We relegate such improvement to future studies.

ACKNOWLEDGMENTS

We are grateful to L. E. Herrera Rodríguez for technical help regarding intricacies of HEOM calculations. F.R.-O., F.G.-G. and B.K.N. were supported by the U.S. National Science Foundation (NSF) under Grant No. DMR-2500816. P.P. was partially supported by the U.S. Army Research Office under Grant No. W911NF-22-2-0234. S.R.C. gratefully acknowledges financial support from UK’s Engineering and Physical Sciences Research Council (EPSRC) under Grant No. EP/T028424/1.

-
- [1] S. Patra, S. Singh, and R. Orús, Projected entangled pair states with flexible geometry, *Phys. Rev. Res.* **7**, L012002 (2025).
 - [2] H.-P. Breuer and F. Petruccione, *The Theory of Open Quantum Systems* (Oxford University Press, Oxford, 2007).
 - [3] V. Reimer, M. R. Wegewijs, K. Nestmann, and M. Pletyukhov, Five approaches to exact open-system dynamics: Complete positivity, divisibility, and time-dependent observables, *J. Chem. Phys.* **151**, 044101 (2019).
 - [4] H.-P. Breuer, E.-M. Laine, J. Piilo, and B. Vacchini, Colloquium: Non-Markovian dynamics in open quantum systems, *Rev. Mod. Phys.* **88**, 021002 (2016).
 - [5] I. de Vega and D. Alonso, Dynamics of non-Markovian open quantum systems, *Rev. Mod. Phys.* **89**, 015001 (2017).
 - [6] G. Lindblad, On the generators of quantum dynamical semigroups, *Commun. Math. Phys.* **48**, 119 (1976).
 - [7] F. Nathan and M. S. Rudner, Universal Lindblad equation for open quantum systems, *Phys. Rev. B* **102**, 115109 (2020).
 - [8] S. Nakajima, On quantum theory of transport phenomena: Steady diffusion, *Prog. Theor. Phys.* **20**, 948 (1958).
 - [9] R. Zwanzig, Ensemble method in the theory of irreversibility, *J. Chem. Phys.* **33**, 1338 (1960).
 - [10] A. Rivas, S. F. Huelga, and M. B. Plenio, Quantum non-Markovianity: characterization, quantification and detection, *Rep. Prog. Phys.* **77**, 094001 (2014).
 - [11] D. Chruściński and A. Kossakowski, Non-Markovian quantum dynamics: Local versus nonlocal, *Phys. Rev. Lett.* **104**, 070406 (2010).
 - [12] K. Nestmann and M. R. Wegewijs, General connection between time-local and time-nonlocal perturbation expansions, *Phys. Rev. B* **104**, 155407 (2021).
 - [13] K. Nestmann, V. Bruch, and M. R. Wegewijs, How quantum evolution with memory is generated in a time-local way, *Phys. Rev. X* **11**, 021041 (2021).

- [14] T. Prosen, Third quantization: a general method to solve master equations for quadratic open Fermi systems, *New J. Phys.* **10**, 043026 (2008).
- [15] A. McDonald and A. A. Clerk, Third quantization of open quantum systems: Dissipative symmetries and connections to phase-space and Keldysh field-theory formulations, *Phys. Rev. Res.* **5**, 033107 (2023).
- [16] A. J. Leggett, S. Chakravarty, A. T. Dorsey, M. P. A. Fisher, A. Garg, and W. Zwerger, Dynamics of the dissipative two-state system, *Rev. Mod. Phys.* **59**, 1 (1987).
- [17] L. E. Ballentine, *Quantum Mechanics: A Modern Development* (World Scientific, Singapore, 2014).
- [18] E. Joos, H. D. Zeh, C. Kiefer, D. Giulini, J. Kupsch, and I.-O. Stamatescu, *Decoherence and the Appearance of a Classical World in Quantum Theory* (Springer, Berlin Heidelberg, 2003).
- [19] M. D. Petrović, P. Mondal, A. E. Feiguin, P. Plecháč, and B. K. Nikolić, Spintronics meets density matrix renormalization group: Quantum spin-torque-driven nonclassical magnetization reversal and dynamical buildup of long-range entanglement, *Phys. Rev. X* **11**, 021062 (2021).
- [20] A. Suresh, R. D. Soares, P. Mondal, J. P. S. Pires, J. M. V. P. Lopes, A. Ferreira, A. E. Feiguin, P. Plecháč, and B. K. Nikolić, Electron-mediated entanglement of two distant macroscopic ferromagnets within a nonequilibrium spintronic device, *Phys. Rev. A* **109**, 022414 (2024).
- [21] S. Kovarik, R. Schlitz, A. Vishwakarma, D. Ruckert, P. Gambardella, and S. Stepanow, Spin torque-driven electron paramagnetic resonance of a single spin in a pentacene molecule, *Science* **384**, 1368 (2024).
- [22] D.-J. Choi, N. Lorente, J. Wiebe, K. von Bergmann, A. F. Otte, and A. J. Heinrich, *Colloquium: Atomic spin chains on surfaces*, *Rev. Mod. Phys.* **91**, 041001 (2019).
- [23] Y. Chen, Y. Bae, and A. J. Heinrich, Harnessing the quantum behavior of spins on surfaces, *Adv. Mater.* **35**, 2107534 (2023).
- [24] F. Thompson and A. Kamenev, Field theory of many-body Lindbladian dynamics, *Ann. Phys.* **455**, 169385 (2023).
- [25] L. M. Sieberer, M. Buchhold, and S. Diehl, Keldysh field theory for driven open quantum systems, *Rep. Prog. Phys.* **79**, 096001 (2016).
- [26] A. Kamenev, *Field Theory of Non-Equilibrium Systems* (Cambridge University Press, Cambridge, 2023).
- [27] J. Berges, Nonequilibrium quantum fields: From cold atoms to cosmology, *arXiv:1503.02907* (2015).
- [28] E. A. Calzetta and B.-L. B. Hu, *Nonequilibrium Quantum Field Theory* (Cambridge University Press, Cambridge, 2008).
- [29] F. Gelis, *Quantum Field Theory: From Basics to Modern Topics* (Cambridge University Press, Cambridge, 2019).
- [30] G. Stefanucci, Kadanoff-Baym equations for interacting systems with dissipative Lindbladian dynamics, *Phys. Rev. Lett.* **133**, 066901 (2024).
- [31] C. Burrage, C. Käding, P. Millington, and J. Minář, Open quantum dynamics induced by light scalar fields, *Phys. Rev. D* **100**, 076003 (2019).
- [32] M. F. Maghrebi and A. V. Gorshkov, Nonequilibrium many-body steady states via Keldysh formalism, *Phys. Rev. B* **93**, 014307 (2016).
- [33] H. Hosseinabadi, D. E. Chang, and J. Marino, Far from equilibrium field theory for strongly coupled light and matter: Dynamics of frustrated multimode cavity QED, *Phys. Rev. Res.* **6**, 043314 (2024).
- [34] C. Müller and T. M. Stace, Deriving Lindblad master equations with Keldysh diagrams: Correlated gain and loss in higher order perturbation theory, *Phys. Rev. A* **95**, 013847 (2017).
- [35] B. Gulácsi and G. Burkard, Signatures of non-Markovianity of a superconducting qubit, *Phys. Rev. B* **107**, 174511 (2023).
- [36] M. Rossini, D. Maile, J. Ankerhold, and B. I. C. Donvil, Single-qubit error mitigation by simulating non-Markovian dynamics, *Phys. Rev. Lett.* **131**, 110603 (2023).
- [37] C. P. Koch, Controlling open quantum systems: tools, achievements, and limitations, *J. Phys.: Condens. Matter* **28**, 213001 (2016).
- [38] P. M. Harrington, E. J. Mueller, and K. W. Murch, Engineered dissipation for quantum information science, *Nat. Rev. Phys.* **4**, 660 (2022).
- [39] G. E. Fux, D. Kilda, B. W. Lovett, and J. Keeling, Tensor network simulation of chains of non-Markovian open quantum systems, *Phys. Rev. Res.* **5**, 033078 (2023).
- [40] G. E. Fux, P. Fowler-Wright, J. Beckles, E. P. Butler, P. R. Eastham, D. Gribben, J. Keeling, D. Kilda, P. Kirtton, E. D. C. Lawrence, *et al.*, OQuPy: A Python package to efficiently simulate non-Markovian open quantum systems with process tensors, *J. Chem. Phys.* **161**, 124108 (2024).
- [41] M. Cygorek and E. M. Gauger, ACE: a general-purpose non-Markovian open quantum systems simulation toolkit based on process tensors, *J. Chem. Phys.* **161**, 074111 (2024).
- [42] Y. Sun, G. Wang, and Z. Cai, Simulation of spin chains with off-diagonal coupling using the inchworm method, *J. Chem. Theory Comput.* **20**, 9321 (2024).
- [43] M. Xu, J. T. Stockburger, and J. Ankerhold, Environment-mediated long-ranged correlations in many-body system, *J. Chem. Phys.* **161**, 124105 (2024).
- [44] D. Rosenberg, D. Kim, R. Das, D. Yost, S. Gustavsson, D. Hover, P. Krantz, A. Melville, L. Racz, G. O. Samach, *et al.*, 3D integrated superconducting qubits, *npj Quantum Inf.* **3**, 42 (2017).
- [45] H. Yuan, Y. Cao, A. Kamra, R. A. Duine, and P. Yan, Quantum magnonics: When magnon spintronics meets quantum information science, *Phys. Rep.* **965**, 1 (2022).
- [46] S. Borsányi, Nonequilibrium field theory from the 2PI effective action, *arXiv:hep-ph/0512308* (2005).
- [47] M. Babadi, E. Demler, and M. Knap, Far-from-equilibrium field theory of many-body quantum spin systems: Prethermalization and relaxation of spin spiral states in three dimensions, *Phys. Rev. X* **5**, 041005 (2015).
- [48] A. Schuckert, A. Orioli, and J. Berges, Nonequilibrium quantum spin dynamics from two-particle irreducible functional integral techniques in the Schwinger boson representation, *Phys. Rev. B* **98**, 224304 (2018).
- [49] M. Brown and I. Whittingham, Two-particle irreducible effective actions versus resummation: Analytic properties and self-consistency, *Nucl. Phys. B* **900**, 477 (2015).
- [50] H. Mera, T. G. Pedersen, and B. K. Nikolić, Nonperturbative quantum physics from low-order perturbation theory, *Phys. Rev. Lett.* **115**, 143001 (2015).

- [51] H. Mera, T. G. Pedersen, and B. K. Nikolić, Hypergeometric resummation of self-consistent sunset diagrams for steady-state electron-boson quantum many-body systems out of equilibrium, *Phys. Rev. B* **94**, 165429 (2016).
- [52] H. Mera, T. G. Pedersen, and B. K. Nikolić, Fast summation of divergent series and resurgent transseries from Meijer- g approximants, *Phys. Rev. D* **97**, 105027 (2018).
- [53] J. M. Cornwall, R. Jackiw, and E. Tomboulis, Effective action for composite operators, *Phys. Rev. D* **10**, 2428 (1974).
- [54] M. Mariño, *Instantons and Large N : An Introduction to Non-Perturbative Methods in Quantum Field Theory* (Cambridge University Press, Cambridge, 2015).
- [55] L. Di Pietro, M. Mariño, G. Sberveglieri, and M. Serone, Resurgence and $1/N$ expansion in integrable field theories, *J. High Energ. Phys.* **2021** (10), 166.
- [56] I. Aniceto, G. Başar, and R. Schiappa, A primer on resurgent transseries and their asymptotics, *Phys. Rep.* **809**, 1 (2019).
- [57] N. Makri, Numerical path integral techniques for long time dynamics of quantum dissipative systems, *J. Math. Phys.* **36**, 2430 (1995).
- [58] A. Winter, H. Rieger, M. Vojta, and R. Bulla, Quantum phase transition in the sub-Ohmic spin-boson model: Quantum Monte Carlo study with a continuous imaginary time cluster algorithm, *Phys. Rev. Lett.* **102**, 030601 (2009).
- [59] A. W. Chin, A. Rivas, S. F. Huelga, and M. B. Plenio, Exact mapping between system-reservoir quantum models and semi-infinite discrete chains using orthogonal polynomials, *J. Math. Phys.* **51**, 092109 (2010).
- [60] H. Wang and M. Thoss, From coherent motion to localization: dynamics of the spin-boson model at zero temperature, *New J. Phys.* **10**, 115005 (2008).
- [61] H. Wang and M. Thoss, From coherent motion to localization: II. dynamics of the spin-boson model with sub-Ohmic spectral density at zero temperature, *Chem. Phys.* **370**, 78 (2010).
- [62] A. Strathearn, B. W. Lovett, and P. Kirton, Efficient real-time path integrals for non-Markovian spin-boson models, *New J. Phys.* **19**, 093009 (2017).
- [63] A. Strathearn, P. Kirton, D. Kilda, J. Keeling, and B. W. Lovett, Efficient non-Markovian quantum dynamics using time-evolving matrix product operators, *Nat. Commun.* **9**, 3322 (2018).
- [64] E. Ye and G. K.-L. Chan, Constructing tensor network influence functionals for general quantum dynamics, *J. Chem. Phys.* **155**, 044104 (2021).
- [65] M. Cygorek, M. Cosacchi, A. Vagov, V. M. Axt, B. W. Lovett, J. Keeling, and E. M. Gauger, Simulation of open quantum systems by automated compression of arbitrary environments, *Nat. Phys.* **18**, 662 (2022).
- [66] M. Weber, Quantum Monte Carlo simulation of spin-boson models using wormhole updates, *Phys. Rev. B* **105**, 165129 (2022).
- [67] I. de Vega and M.-C. Bañuls, Thermofield-based chain-mapping approach for open quantum systems, *Phys. Rev. A* **92**, 052116 (2015).
- [68] R. Bulla, N.-H. Tong, and M. Vojta, Numerical renormalization group for bosonic systems and application to the sub-Ohmic spin-boson model, *Phys. Rev. Lett.* **91**, 170601 (2003).
- [69] F. B. Anders and A. Schiller, Spin precession and real-time dynamics in the Kondo model: Time-dependent numerical renormalization-group study, *Phys. Rev. B* **74**, 245113 (2006).
- [70] F. B. Anders, R. Bulla, and M. Vojta, Equilibrium and nonequilibrium dynamics of the sub-Ohmic spin-boson model, *Phys. Rev. Lett.* **98**, 210402 (2007).
- [71] M. Vojta, Numerical renormalization group for the sub-Ohmic spin-boson model: A conspiracy of errors, *Phys. Rev. B* **85**, 115113 (2012).
- [72] P. P. Orth, A. Imambekov, and K. Le Hur, Nonperturbative stochastic method for driven spin-boson model, *Phys. Rev. B* **87**, 014305 (2013).
- [73] I. Vilkoviskiy and D. A. Abanin, Bound on approximating non-Markovian dynamics by tensor networks in the time domain, *Phys. Rev. B* **109**, 205126 (2024).
- [74] O. Scarlatella and M. Schirò, Self-consistent dynamical maps for open quantum systems, *SciPost Phys.* **16**, 026 (2024).
- [75] F. Ivander, L. P. Lindoy, and J. Lee, Unified framework for open quantum dynamics with memory, *Nat. Commun.* **15**, 8087 (2024).
- [76] M. Xu and J. Ankerhold, About the performance of perturbative treatments of the spin-boson dynamics within the hierarchical equations of motion approach, *Eur. Phys. J. Spec. Top.* **232**, 3209–3217 (2023).
- [77] M. Xu, V. Vadimov, M. Krug, J. T. Stockburger, and J. Ankerhold, A universal framework for quantum dissipation: Minimally extended state space and exact time-local dynamics, *arXiv:2307.16790* (2023).
- [78] F. Shibata and T. Arimitsu, Expansion formulas in nonequilibrium statistical mechanics, *J. Phys. Soc. Japan* **49**, 891 (1980).
- [79] Y. Tanimura, Numerically “exact” approach to open quantum dynamics: The hierarchical equations of motion (HEOM), *J. Chem. Phys.* **153**, 020901 (2020).
- [80] G. Clos and H.-P. Breuer, Quantification of memory effects in the spin-boson model, *Phys. Rev. A* **86**, 012115 (2012).
- [81] S. Wenderoth, H.-P. Breuer, and M. Thoss, Non-Markovian effects in the spin-boson model at zero temperature, *Phys. Rev. A* **104**, 012213 (2021).
- [82] M. Xu, Y. Yan, Q. Shi, J. Ankerhold, and J. T. Stockburger, Taming quantum noise for efficient low temperature simulations of open quantum systems, *Phys. Rev. Lett.* **129**, 230601 (2022).
- [83] M. Xu, L. Song, K. Song, and Q. Shi, Convergence of high order perturbative expansions in open system quantum dynamics, *J. Chem. Phys.* **146**, 064102 (2017).
- [84] J. Haegeman, C. Lubich, I. Oseledets, B. Vandereycken, and F. Verstraete, Unifying time evolution and optimization with matrix product states, *Phys. Rev. B* **94**, 165116 (2016).
- [85] T. Chanda, P. Sierant, and J. Zakrzewski, Time dynamics with matrix product states: Many-body localization transition of large systems revisited, *Phys. Rev. B* **101**, 035148 (2020).
- [86] N. Ng, G. Park, A. J. Millis, G. K.-L. Chan, and D. R. Reichman, Real-time evolution of Anderson impurity models via tensor network influence functionals, *Phys. Rev. B* **107**, 125103 (2023).
- [87] J. Thoenniss, M. Sonner, A. Leroose, and D. A. Abanin, Efficient method for quantum impurity problems out of equilibrium, *Phys. Rev. B* **107**, L201115 (2023).

- [88] F. A. Pollock, C. Rodríguez-Rosario, T. Frauenheim, M. Paternostro, and K. Modi, Non-Markovian quantum processes: Complete framework and efficient characterization, *Phys. Rev. A* **97**, 012127 (2018).
- [89] S. Milz and K. Modi, Quantum stochastic processes and quantum non-Markovian phenomena, *PRX Quantum* **2**, 030201 (2021).
- [90] A. Lerose, M. Sonner, and D. A. Abanin, Overcoming the entanglement barrier in quantum many-body dynamics via space-time duality, *Phys. Rev. B* **107**, L060305 (2023).
- [91] M. M. Rams and M. Zwolak, Breaking the entanglement barrier: Tensor network simulation of quantum transport, *Phys. Rev. Lett.* **124**, 137701 (2020).
- [92] A. Foligno, T. Zhou, and B. Bertini, Temporal entanglement in chaotic quantum circuits, *Phys. Rev. X* **13**, 041008 (2023).
- [93] F. Garcia-Gaitan and B. K. Nikolić, Fate of entanglement in magnetism under Lindbladian or non-Markovian dynamics and conditions for their transition to Landau-Lifshitz-Gilbert classical dynamics, *Phys. Rev. B* **109**, L180408 (2024).
- [94] R. Trivedi and J. I. Cirac, Transitions in computational complexity of continuous-time local open quantum dynamics, *Phys. Rev. Lett.* **129**, 260405 (2022).
- [95] M. P. Woods, M. Cramer, and M. B. Plenio, Simulating bosonic baths with error bars, *Phys. Rev. Lett.* **115**, 130401 (2015).
- [96] M. P. Woods and M. B. Plenio, Dynamical error bounds for continuum discretisation via Gauss quadrature rules—A Lieb-Robinson bound approach, *J. Math. Phys.* **57**, 022105 (2016).
- [97] U. Bajpai, A. Suresh, and B. K. Nikolić, Quantum many-body states and Green's functions of nonequilibrium electron-magnon systems: Localized spin operators versus their mapping to Holstein-Primakoff bosons, *Phys. Rev. B* **104**, 184425 (2021).
- [98] A. Auerbach, *Interacting Electrons and Quantum Magnetism* (Springer, New York, 1994).
- [99] S.-S. Zhang, E. A. Ghioldi, L. O. Manuel, A. E. Trumper, and C. D. Batista, Schwinger boson theory of ordered magnets, *Phys. Rev. B* **105**, 224404 (2022).
- [100] M. Gohlke, A. Corticelli, R. Moessner, P. A. McClarty, and A. Mook, Spurious symmetry enhancement in linear spin wave theory and interaction-induced topology in magnons, *Phys. Rev. Lett.* **131**, 186702 (2023).
- [101] Q.-S. Li, H.-Y. Liu, Q. Wang, Y.-C. Wu, and G.-P. Guo, A unified framework of transformations based on the Jordan-Wigner transformation, *J. Chem. Phys.* **157**, 134104 (2022).
- [102] G. Stefanucci and R. van Leeuwen, *Nonequilibrium Many-Body Theory of Quantum Systems: A Modern Introduction* (Cambridge University Press, Cambridge, 2025).
- [103] N. Schlünzen, S. Hermanns, M. Scharnke, and M. Bonitz, Ultrafast dynamics of strongly correlated fermions—nonequilibrium Green functions and self-energy approximations, *J. Phys.: Condens. Matter* **32**, 103001 (2019).
- [104] A. Altland and B. Simons, *Condensed Matter Field Theory* (Cambridge University Press, Cambridge, 2023).
- [105] F. Reyes-Osorio and B. K. Nikolić, Gilbert damping in metallic ferromagnets from Schwinger-Keldysh field theory: Intrinsically nonlocal, nonuniform, and made anisotropic by spin-orbit coupling, *Phys. Rev. B* **109**, 024413 (2024).
- [106] J. Anders, C. R. J. Sait, and S. A. R. Horsley, Quantum Brownian motion for magnets, *New J. Phys.* **24**, 033020 (2022).
- [107] R. C. Verstraten, T. Ludwig, R. A. Duine, and C. Morais Smith, Fractional Landau-Lifshitz-Gilbert equation, *Phys. Rev. Res.* **5**, 033128 (2023).
- [108] M. Thomas, T. Karzig, S. V. Kusminskiy, G. Zaránd, and F. von Oppen, Scattering theory of adiabatic reaction forces due to out-of-equilibrium quantum environments, *Phys. Rev. B* **86**, 195419 (2012).
- [109] U. Bajpai and B. Nikolić, Time-retarded damping and magnetic inertia in the Landau-Lifshitz-Gilbert equation self-consistently coupled to electronic time-dependent nonequilibrium Green functions, *Phys. Rev. B* **99**, 134409 (2019).
- [110] L. M. Sieberer, S. D. Huber, E. Altman, and S. Diehl, Dynamical critical phenomena in driven-dissipative systems, *Phys. Rev. Lett.* **110**, 195301 (2013).
- [111] J. Rammer, *Quantum Field Theory of Non-equilibrium States* (Cambridge University Press, Cambridge, 2007).
- [112] J. Berges, Controlled nonperturbative dynamics of quantum fields out of equilibrium, *Nucl. Phys. A* **699**, 847 (2002).
- [113] G. Aarts and J. Berges, Classical aspects of quantum fields far from equilibrium, *Phys. Rev. Lett.* **88**, 041603 (2002).
- [114] A. M. Rey, B. L. Hu, E. Calzetta, A. Roura, and C. W. Clark, Nonequilibrium dynamics of optical-lattice-loaded Bose-Einstein-condensate atoms: Beyond the Hartree-Fock-Bogoliubov approximation, *Phys. Rev. A* **69**, 033610 (2004).
- [115] A. G. Burchards, J. Feldmeier, A. Schuckert, and M. Knap, Coupled hydrodynamics in dipole-conserving quantum systems, *Phys. Rev. B* **105**, 205127 (2022).
- [116] M. Kronenwett and T. Gasenzer, Far-from-equilibrium dynamics of an ultracold Fermi gas, *Appl. Phys. B* **102**, 469 (2011).
- [117] S. Takei, Spin transport in an electrically driven magnon gas near Bose-Einstein condensation: Hartree-Fock-Keldysh theory, *Phys. Rev. B* **100**, 134440 (2019).
- [118] F. Mahfouzi and B. K. Nikolić, Signatures of electron-magnon interaction in charge and spin currents through magnetic tunnel junctions: A nonequilibrium many-body perturbation theory approach, *Phys. Rev. B* **90**, 045115 (2014).
- [119] L. Kantorovich, Generalized Langreth rules, *Phys. Rev. B* **101**, 165408 (2020).
- [120] F. Meirinhos, M. Kajan, J. Kroha, and T. Bode, Adaptive numerical solution of Kadanoff-Baym equations, *SciPost Phys. Core* **5**, 030 (2022).
- [121] L. Savary and L. Balents, Quantum spin liquids: a review, *Rep. Prog. Phys.* **80**, 016502 (2016).
- [122] G. Vidal, Efficient classical simulation of slightly entangled quantum computations, *Phys. Rev. Lett.* **91**, 147902 (2003).
- [123] Y. Takahashi and H. Umezawa, Thermo field dynamics, *Int. J. Mod. Phys. B* **10**, 1755 (1996).
- [124] W. Gautschi, Orthogonal polynomials (in Matlab), *J. Comput. Appl. Math.* **178**, 215 (2005).
- [125] J. Haegeman, J. I. Cirac, T. J. Osborne, I. Pizorn, H. Verschelde, and F. Verstraete, Time-dependent variational principle for quantum lattices, *Phys. Rev. Lett.*

- [107, 070601 \(2011\)](#).
- [126] J. Haegeman, C. Lubich, I. Oseledets, B. Vandereycken, and F. Verstraete, Unifying time evolution and optimization with matrix product states, *Phys. Rev. B* **94**, 165116 (2016).
 - [127] C. Lubich, I. V. Oseledets, and B. Vandereycken, Time integration of tensor trains, *SIAM J. Numer. Anal.* **53**, 917 (2015).
 - [128] S. Paeckel, T. Köhler, A. Swoboda, S. R. Manmana, U. Schollwöck, and C. Hubig, Time-evolution methods for matrix-product states, *Ann. Phys.* **411**, 167998 (2019).
 - [129] Y. Tanimura and P. G. Wolynes, Quantum and classical Fokker-Planck equations for a Gaussian-Markovian noise bath, *Phys. Rev. A* **43**, 4131 (1991).
 - [130] Y.-T. Huang, P.-C. Kuo, N. Lambert, M. Cirio, S. Cross, S.-L. Yang, F. Nori, and Y.-N. Chen, An efficient Julia framework for hierarchical equations of motion in open quantum systems, *Commun. Phys.* **6**, 313 (2023).
 - [131] C. Meier and D. Tannor, Non-Markovian evolution of the density operator in the presence of strong laser fields, *J. Chem. Phys.* **111**, 3365 (1999).
 - [132] N. Lambert, T. Raheja, S. Cross, P. Menczel, S. Ahmed, A. Pitchford, D. Burgarth, and F. Nori, QuTiP-BoFiN: A bosonic and fermionic numerical hierarchical equations-of-motion library with applications in light-harvesting, quantum control, and single-molecule electronics, *Phys. Rev. Res.* **5**, 013181 (2023).
 - [133] J. Johansson, P. Nation, and F. Nori, QuTiP: An open-source Python framework for the dynamics of open quantum systems, *Comput. Phys. Commun.* **183**, 1760 (2012).
 - [134] J. Johansson, P. Nation, and F. Nori, QuTiP 2: A Python framework for the dynamics of open quantum systems, *Comput. Phys. Commun.* **184**, 1234 (2013).
 - [135] J. F. Koksma, T. Prokopec, and M. G. Schmidt, Decoherence in an interacting quantum field theory: Thermal case, *Phys. Rev. D* **83**, 085011 (2011).
 - [136] K. L. Hur, Entanglement entropy, decoherence, and quantum phase transitions of a dissipative two-level system, *Ann. Phys.* **323**, 2208–2240 (2008).
 - [137] G. De Filippis, A. de Candia, L. M. Cangemi, M. Sassetti, R. Fazio, and V. Cataudella, Quantum phase transitions in the spin-boson model: Monte Carlo method versus variational approach à la Feynman, *Phys. Rev. B* **101**, 180408 (2020).
 - [138] S. Sachdev, *Quantum Phase Transitions* (Cambridge University Press, 2011).
 - [139] M. Weber, D. J. Luitz, and F. F. Assaad, Dissipation-induced order: The $s = 1/2$ quantum spin chain coupled to an Ohmic bath, *Phys. Rev. Lett.* **129**, 056402 (2022).
 - [140] K. Yang, S. C. Morampudi, and E. J. Bergholtz, Exceptional spin liquids from couplings to the environment, *Phys. Rev. Lett.* **126**, 077201 (2021).
 - [141] A. Scheie, P. Laurell, A. M. Samarakoon, B. Lake, S. E. Nagler, G. E. Granroth, S. Okamoto, G. Alvarez, and D. A. Tennant, Witnessing entanglement in quantum magnets using neutron scattering, *Phys. Rev. B* **103**, 224434 (2021).
 - [142] G. T. Landi, D. Poletti, and G. Schaller, Nonequilibrium boundary-driven quantum systems: Models, methods, and properties, *Rev. Mod. Phys.* **94**, 045006 (2022).
 - [143] F. Göhmann, K. K. Kozłowski, J. Sirker, and J. Suzuki, Spin conductivity of the XXZ chain in the antiferromagnetic massive regime, *SciPost Phys.* **12**, 158 (2022).
 - [144] J. J. Mendoza-Arenas, S. Al-Assam, S. R. Clark, and D. Jaksch, Heat transport in the XXZ spin chain: from ballistic to diffusive regimes and dephasing enhancement, *J. Stat. Mech.* **2013**, P07007 (2013).
 - [145] L. Del Re, B. Rost, A. F. Kemper, and J. K. Freericks, Driven-dissipative quantum mechanics on a lattice: Simulating a fermionic reservoir on a quantum computer, *Phys. Rev. B* **102**, 125112 (2020).
 - [146] A. S. Nikolaeva, E. O. Kiktenko, and A. K. Fedorov, Efficient realization of quantum algorithms with qudits, *EPJ Quantum Technol.* **11**, 43 (2024).
 - [147] N. Schlünzen, J.-P. Joost, F. Heidrich-Meisner, and M. Bonitz, Nonequilibrium dynamics in the one-dimensional Fermi-Hubbard model: Comparison of the nonequilibrium Green-functions approach and the density matrix renormalization group method, *Phys. Rev. B* **95**, 165139 (2017).
 - [148] M. Cygorek, J. Keeling, B. W. Lovett, and E. M. Gauger, Sublinear scaling in non-Markovian open quantum systems simulations, *Phys. Rev. X* **14**, 011010 (2024).
 - [149] E. Stoudenmire and S. R. White, Studying two-dimensional systems with the density matrix renormalization group, *Annu. Rev. Condens. Matter Phys.* **3**, 111 (2012).
 - [150] J. I. Cirac, D. Pérez-García, N. Schuch, and F. Verstraete, Matrix product states and projected entangled pair states: Concepts, symmetries, theorems, *Rev. Mod. Phys.* **93**, 045003 (2021).
 - [151] J. Berges, n -particle irreducible effective action techniques for gauge theories, *Phys. Rev. D* **70**, 105010 (2004).
 - [152] M. E. Carrington, B. A. Meggison, and D. Pickering, 2PI effective action at four loop order in φ^4 theory, *Phys. Rev. D* **94**, 025018 (2016).
 - [153] M. Gorny and M. M. Müller, Kadanoff-Baym equations with non-Gaussian initial conditions: The equilibrium limit, *Phys. Rev. D* **80**, 085011 (2009).